NASA
Technical
Paper
2863

November 1988

Indentation Plasticity and Fracture in Silicon

George C. Rybicki
and P. Pirouz

NASA

NASA
Technical
Paper
2863

1988

Indentation Plasticity and Fracture in Silicon

George C. Rybicki
Lewis Research Center
Cleveland, Ohio

P. Pirouz
Case Western Reserve University
Cleveland, Ohio

National Aeronautics
and Space Administration

**Scientific and Technical
Information Division**

Summary

Measurements of the ductile-brittle transition temperature (DBTT) of heavily doped silicon were obtained by using indentation techniques. Diamond pyramid hardness tests were performed on the (100) face of heavily doped *n*-type and *p*-type and intrinsic silicon single crystals. Tests were performed at 200 to 850 °C with loads of 100 to 500 g. Samples were subsequently etched to reveal dislocation rosettes produced by indentation.

Intrinsic silicon underwent a ductile-brittle transition at 660 °C, *p*-type at 645 °C, and *n*-type at 625 °C. Hardness values varied from 1.1 GPa at 700 °C to 11.7 GPa at 200 °C. Significant effects of hardness on doping were present only at the highest temperatures. Lower loads generally produced higher hardness, but load did not affect the DBTT. Fracture toughness values ranged from 0.9 MPa $m^{1/2}$ at 200 °C to 2.75 MPa $m^{1/2}$ near the DBTT. Doping did not affect the fracture toughness of silicon. The *p*-type doping increased the size of dislocation rosettes observed after indentation, but the *n*-type did not, in contradiction of the expected results. Results are discussed in terms of the effect of doping on the dislocation mobility in silicon.

Introduction

Doping of semiconductors is commonly performed to alter the electrical properties and to facilitate device construction. Recently it has been demonstrated that such doping can also affect the mechanical properties of these materials. Several authors have worked in this area, and theories for the effect have been proposed. Research in this area has been very difficult to perform, and the availability of research materials was limited. Today very high purity silicon is available with heavy doping to facilitate the observation of these effects. It has also been demonstrated that this effect can be observed through the simple microhardness test if the test can be performed over a range of temperatures. This equipment is now commercially available.

Elucidation of these effects could be of great value to the semiconductor manufacturing technologies where doping may affect machining processes or device fabrication. These effects may also be important in the study of fracture in SiC, a high-temperature structural material and a semiconductor.

In the present study the ductile-brittle transition of doped and undoped silicon was studied by hot microhardness testing. Dislocation mobility was studied by etch pitting, and hardness and fracture toughness were calculated at various temperatures. The results are discussed in terms of the theories proposed.

Theory

Indentation Hardness and Analysis

The measurement of the hardness of materials is a well-developed technique of long standing and great value in materials science. The earliest measurements of hardness were based on one material's ability to scratch another. Modern hardness testing has attained much greater sophistication. Today hardness testing is used in quality control and research and can be used to determine hardness, yield strength, and fracture toughness of a material. Some of the great advantages of hardness testing include simple sample preparation, small sample volume, and the test's nondestructive nature.

The most common types of hardness testing involve the application of a measured load to a sample with an indenter of hardness significantly greater than that of the material being evaluated. In the Brinell test, a steel or tungsten carbide ball is pressed against the surface of the material, and the residual impression is measured. The hardness is reported as a function of load over surface area of the indent.

$$\mathrm{BHN} = \frac{P}{\pi D t} = \frac{P}{(\pi/2)D^2(1 - \cos\theta)}$$

where BHN is Brinell hardness, P is the load in kg, D is the ball diameter in mm, t is the depth of the impression, and θ is the included angle. The term θ relates the depth of the impression to its diameter and thus can introduce an effect of impression size to load. This can lead to a variance of hardness with applied load. Despite this limitation Brinell hardness is a valuable tool and is widely used in industry today. The Brinell hardness of a metal can be related to its ultimate tensile strength (UTS) by using the equation UTS = 470 BHN. The constant 470 applies to non-strain-hardening materials, whereas 500 is the constant for steels. This effect must be considered when using these relationships.

The large size of the Brinell indenter is also useful in averaging out local inhomogeneities, and the sample preparation can be as simple as grinding a flat spot on the piece to be tested.

A similar test is the Rockwell hardness test. In the Rockwell test a semipointed diamond or small-diameter carbide ball is used as an indenter. A variety of loads may be used, from 60 to 160 kg. In this hardness test a 10-kg preload seats the specimen, and the type of indenter and load are selected to fit the range of hardness expected. The hardness is reported on a scale of 0 to 100 based on a surface penetration of 0.0008 in. This method eliminates the chance of operator interpretation errors, but the hardness numbers have no physical basis. The main disadvantage of the Rockwell test is that one hardness scale is insufficient to cover all materials. This method requires only a small sample and lends itself nicely to production environments. Rockwell measurements can be converted or compared with Brinell or other hardness measurements, but this can introduce error if not done carefully.

One of the most useful tests is the diamond pyramid, or Vickers hardness test (DPH). In this test the indenter is a small diamond pyramid with an angle of 136° between the faces. This test produces indents that are geometrically similar regardless of load and eliminates the variation of hardness with load, except with very small loads (ref. 1). Hardness is calculated as load over surface area of the indent:

$$\mathrm{DPH} = 1.854\,\frac{P}{L^2}$$

where L is the indentation diagonal and P is the load. In this test, by varying load from 10 g to 10 kg one scale can be used for all materials. The hardness H can be related to the yield strength of the material σ_y by using the equation $H = 2.78\,\sigma_y$ for non-strain-hardening materials. The microhardness test is usually performed with the aid of a microscope, and only a very small specimen is required.

One of the major advantages of the microhardness test is that the indentation process imposes a considerable hydrostatic stress on the material. This is a great advantage when testing brittle materials. The hydrostatic pressure suppresses fracture and makes an otherwise difficult measurement routine. In other types of mechanical tests such as bend or tensile testing careful machining is required so that surface defects do not create stress raisers and affect the test. The microhardness test also eliminates the difficulties associated with machine and fixture alignment.

There are some drawbacks to the microhardness test. Errors produced by sinking-in of the diamond on soft materials can lead to overestimation of the diagonal length. On the other hand, recovery of the indentation at low loads can lead to underestimation of the hardness. In testing brittle materials, cracking can make the interpretation of results difficult. Of course, errors can be introduced by the operator.

Another technique for microhardness testing is the Knoop test. A long, thin pyramid with a length-to-width ratio of 7 to 1 is used as an indenter in this test. The indent produced reduces the effects of recovery found in the Vickers test because the long diagonal is affected very little by recovery. The narrow indent produced is useful in testing thin areas and in evaluating any hardness anisotropy present in a material. The analysis is similar to that of the Vickers test.

Stress Field Around Indentations

The stress field around an indentation was analyzed by Yoffe (ref. 2). The resulting stress field is a combination of the Boussinesq solution for a point load and the blister field for the plastic deformation. The following equations describe the field:

$$\sigma_r = \frac{P}{4\pi r^2}(1 - 7\cos\theta) + \frac{\mathrm{B}}{r^3}(19\cos^2\theta - 7)$$

$$\sigma_\theta = \frac{P}{4\pi r^2}\frac{\cos^2\theta}{(1 + \cos\theta)} - \frac{\mathrm{B}}{r^3}\cos^2\theta$$

$$\sigma_\phi = \frac{P}{4\pi r^2}\left(\cos\theta - \frac{1}{1 + \cos\theta}\right) + \frac{\mathrm{B}}{r^3}(2 - 3\cos^2\theta)$$

$$\tau = \frac{P}{4\pi r^2}\frac{\sin\theta\cos\theta}{1 - \cos\theta} + \frac{\mathrm{B}}{r^3}5\sin\theta\cos\theta$$

where σ_r is the stress as a function of radial distance r from the indent, σ_θ is the stress as a function of angle θ below the surface, σ_ϕ is the stress as a function of angle ϕ around the indent parallel to the surface, τ is the shear stress, and B is a constant, dependent on the amount of plastic deformation produced during indentation. The coordinate system is shown in figure 1.

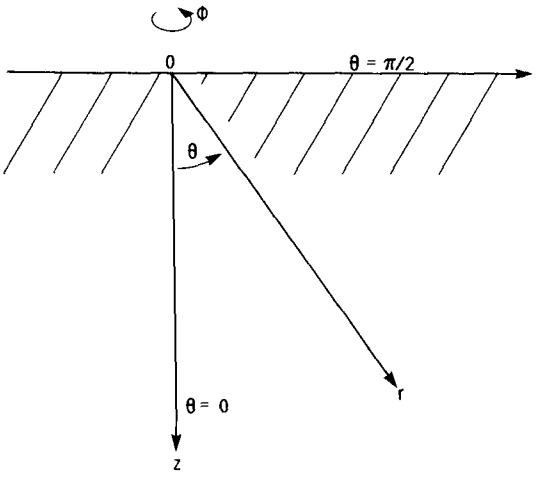

Figure 1.—Coordinate system for stress analysis around indent (from ref. 2).

From this analysis several important conclusions can be drawn. First, stress is dependent on the load and on $1/r^2$. Second, maxima in the tensile stress occur at $\theta = 0$, where median cracks form, and at $\theta = \pi/2$, where a ring crack can form. From the blister field analysis it can be seen that residual stresses of a tensile nature form upon unloading; these stresses can drive median cracks to the surface. Lastly, upon unloading, continuity in normal and shear stresses must be maintained across the boundary between the plastic and elastic zones but not parallel to it. Therefore a large tensile stress may be present parallel to this boundary, and this is where lateral cracks can occur (ref. 2).

The size of the plastic zone formed by indentation has been described in terms of the ratio of the plastic zone size to the indent size

$$\left(\frac{R_p}{R_i}\right)^3 = \frac{E}{3\sigma_y(1-\nu)}$$

where R_i is the indent radius, R_p is the plastic zone radius, E is the Youngs's modulus, σ_y is the yield stress, and ν is Poisson's ratio (ref. 3). This relationship predicts a ratio of plastic zone to indent diameter of 1.5 to 2.5 to 1 over the temperature range studied here.

The measurement of hardness can be complicated by recovery of the indentation. Breval and MacMillan (ref. 4) have analyzed recovery at the indent. Their analysis yields the relation

$$\left(\frac{Z_r}{a}\right)^2 = 0.08168\left[18.7\left(\frac{H}{E}\right) + 14.03\left(\frac{H}{E}\right)^2\right]$$

where Z_r is the recovered indent depth, a is the recovered indent radius, and H is the hardness. This relation predicts a Z_r/a ratio of 0.212 in silicon at room temperature, and lower values at higher temperatures.

Fracture Around Indentations

Cracking and fractures around the indent can affect the accuracy of microhardness measurements. The energy absorbed by plastic deformation far exceeds that released by cracking for many materials (ref. 5). Although it can make accurate measurements difficult, indentation cracking can reveal important material parameters. Palmqvist was the first to realize that this indentation cracking was related to the fracture toughness of the material (ref. 6).

Because cracks are formed around microhardness indents in several ways, different methods are needed to analyze them. The cracks can be one of two basic types: median and lateral. Median cracks, which form on loading, are deep halfpenny-shaped cracks with the fracture plane normal to the surface. Lateral cracks, which form on unloading, are shallow cracks with a fracture plane approximately parallel to the surface. Lateral cracks are also known as Palmqvist cracks.

A lateral crack is formed as a result of plastic/elastic mismatch stresses. This crack nucleates at the high stress boundary between the zone of plastically deformed material and the elastic region outside of it. As the indenter is removed and the material relaxes, stresses at this boundary reach a value high enough to form a flaw, or to activate an existing flaw, and the crack propagates toward the surface. Niihara (ref. 7) proposed a method by which theses cracks can be used to determine the fracture toughness of a material:

$$\left(\frac{3K_{1c}}{Ha^{1/2}}\right)\left(\frac{H}{3E}\right)^{2/5} = 0.035\left(\frac{l}{a}\right)^{-1/2}$$

where l is the crack length, a is the indentation radius, and K_{1c} is the fracture toughness. Figure 2(a) is the lateral crack geometry.

The median cracks form on planes of maximum stress below the indenter. On loading, the stress reaches a value large enough to activate an existing flaw, or to cause a flaw to form, and a crack propagates. When the load is removed, the residual stress drives the crack through to the surface. Evans and

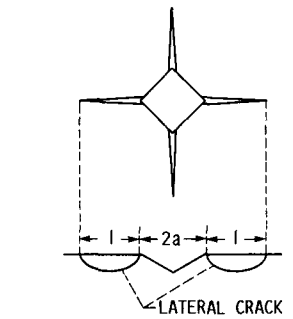

(a)

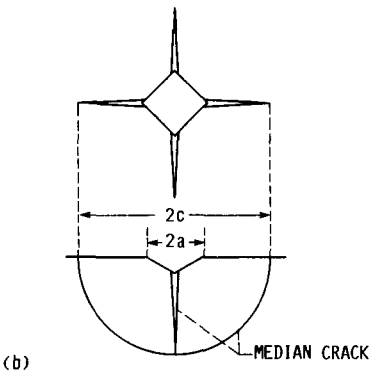

(b)

(a) Lateral crack.
(b) Median crack.

Figure 2.—Lateral and median crack geometry (from ref. 7), where l is crack length, a is indentation radius, and c is crack radius.

Charles (ref. 8) analyzed median crack formation and developed the following relation:

$$\left(\frac{3K_{1c}}{Ha^{1/2}}\right)\left(\frac{H}{3E}\right)^{2/3} = 0.129\left(\frac{c}{a}\right)^{-3/2}$$

where a is indentation radius and c is crack radius. The median crack geometry is shown in figure 2(b). An important point to emerge from these analyses is that the crack length is proportional to load to the ⅔ power in the case of median cracks, and to the ½ power in lateral cracks. This method (ref. 8) is the most popular one used when determining fracture toughness by microhardness indentation.

The hardness and fracture toughness of silicon have been studied extensively. Danyluk, Lim, and Kalejs (ref. 9) studied the hardness of oxygen and carbon-doped silicon. They report hardness values of 12 to 15 GPa, respectively. Lawn and Marshall (ref. 10) report a hardness of 10 GPa and a fracture toughness of 0.6 MPa $m^{1/2}$. Anstis et al. (ref. 11) report a hardness value of 10.6 GPa, and a fracture toughness value of 0.7 MPa $m^{1/2}$. They measured modulus of silicon in four-point bending and report a value of 168 GPa. All the previous results were obtained at room temperature. Roberts, Pirouz, and Hirsch (ref. 12) studied the hardness of n-type, p-type, and intrinsic silicon and found that in both float-zone and Czochralski (CZ) silicon, microhardness is relatively insensitive to doping through 400 °C.

Study of Dislocation Phenomena by Microhardness

Although hardness testing is usually employed to determine the hardness or fracture toughness of a material, it may also be used to investigate related phenomena. Microhardness testing can be used to investigate dislocation mobility, or by using a hot microhardness tester, the ductile-brittle transition temperature (DBTT) for a material displaying this behavior may be determined.

Just as microhardness testing simplifies obtaining the strength and fracture properties of a material, it also simplifies dislocation mobility studies. A typical nonmicrohardness method involves generating dislocation sources in a material (e.g., by a scratch) and applying successive stress pulses. Since the dislocation moves during the time at which the stress is applied, measurement of the successive dislocation positions, by chemical etching, gives the dislocation velocity. This is known as the double etch pit technique. This method is as difficult as mechanical bend testing and has all the complexities. Another traditional method, Lang topography, is used to dynamically measure the velocity of dislocations. This technique, which is based on an x-ray method, is limited to thin specimens, and requires long exposures and intense radiation sources. Qualitative measure of dislocation mobility can be made easily and rapidly by using microindentation test methods.

Hot microhardness testing was used to investigate dislocation mobility in silicon and germanium (ref. 12). High-purity, dislocation-free single crystals of these materials are available, and they can easily be prepared and indented. After indenting, etching with an appropriate etchant reveals arrays of dislocations generated by indenting. The extent of these arrays, called rosettes, can reveal information about dislocation mobility. This technique was used in reference 12 to compare dislocation mobility in doped crystals of float-zone and CZ silicon. Doping with acceptor or donor type impurities produced rosettes of larger diameter than in intrinsic silicon. This implies enhanced dislocation mobility. Float-zone materials also displayed larger rosettes than CZ materials because of lower oxygen content. Oxygen has been known to hinder dislocation mobility in silicon (ref. 13).

Dislocation Mobility in the Diamond Cubic Structure

Silicon and germanium are materials that exist in the diamond cubic structure. This structure can be thought of as a face-centered cubic (fcc) lattice with two atoms per lattice point, one at (0,0,0) and the other at (¼, ¼, ¼) (ref. 14). These materials are covalently bonded and have a large Peierls stress. They are brittle at room temperature.

Dislocations in silicon are similar to those in fcc materials, but at low temperatures, the high Peierls stress confines them largely to the ⟨110⟩ valleys. At low temperature, slip occurs on {111} planes in the ⟨110⟩ directions with Burgers vector 1/2⟨110⟩. Three types of dislocations are predominantly observed: a screw dislocation and two 60° dislocations, although at high temperatures, a pure edge dislocation and others may be observed. Dislocations in silicon are shown to be dissociated in most cases (ref. 15). The screw dislocation dissociates into two 30° partials, and the 60° dislocation dissociates into an edge dislocation (90°) and a 30° partial (ref. 15).

These dislocations may occur on the widely spaced shuffle planes or on the narrowly spaced glide planes. The slip configuration is shown in figure 3, projected along the ⟨110⟩ direction. To form a dislocation in the shuffle configuration requires the removal of a half plane along path 1234. This results in the formation of one dangling bond, which is normal to the glide plane. Formation of a dislocation in the glide

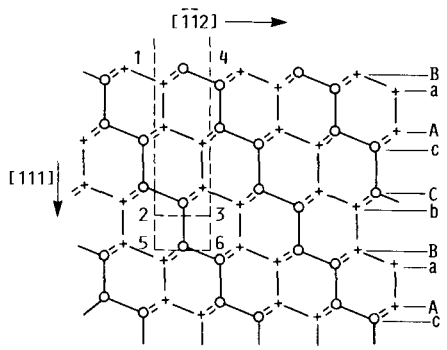

Figure 3.—Diamond cubic lattice projected onto (1̄10) plane. Circles represent atoms in plane of paper; crosses represent atoms in plane below (from ref. 14).

configuration requires the removal of a half plane along 1564. This results in the formation of three dangling bonds, but they are at a small angle to the glide plane. This shallow angle makes it possible for the glide set dangling bonds to reconstruct easily, thus lowering the dislocation energy. Reconstruction of the shuffle set dangling bonds would require much larger displacements. Recent work suggests that the dislocations lie in the glide configuration (ref. 16). It is energetically favorable for the 30° partial to reconstruct, but the results are not clear for the 90° partial (ref. 16). Either configuration gives rise to energy levels in the band gap caused by dangling bonds or dilational strain (ref. 16). Kinks may also be associated with dangling bonds and give rise to levels in the band gap.

Partial dislocations have been observed to move together in silicon but to have differing mobility. This can lead to a large nonequilibrium spacing of the partials (ref. 17). The mobility of the dislocations depends on which partial is leading and which is trailing. Wessel and Alexander (ref. 18) report that the mobilities are

$$90^\circ_t > 90^\circ_l > 30^\circ_l > 30^\circ_t$$

where 90° and 30° refer to the dislocation type and l or t refer to whether that partial is leading or trailing. The observation can be rationalized by considering that reconstruction has occurred in some of the partials, and by considering that the lead partial moves into a perfect lattice, while the trailing partial moves into a stacking fault (ref. 17).

The effect of doping on dislocation mobility was first demonstrated by Patel and Chaudhuri in 1966 (ref. 19). Since this pioneering work, the phenomenon has been studied intensively in silicon (refs. 11 and 20), in germanium (ref. 21), and in compound semiconductors such as gallium arsenide (ref. 22).

Several theories for the effect of doping on dislocation mobility have been proposed. These theories are reviewed in reference 16. The basis of the theories is that dislocation motion in silicon is controlled by the nucleation and motion of kinks. This is known as the drift model and is applicable at high temperatures and low stresses.

The theory of Frisch and Patel (ref. 23) assumes that dislocation velocity is proportional to the number of charged sites on the dislocation line. The Fermi level in this case is calculated by assuming charge neutrality in a cylinder of radius equal to the Debye length surrounding the dislocation. For silicon this would require a change of dislocation charge with p- or n-type doping. The theory does not provide any macroscopic mechanism by which the velocity change can be described.

The theory of Haasen (ref. 24) assumes that the dislocation possesses a line charge q, which lowers the electrostatic energy required to form a double kink. The magnitude of the charge (and thus the effect) is proportional to the Fermi level and to the dislocation donor and acceptor levels in the material.

$$\Delta E = \left(\frac{2q^2h}{e}\right) \exp\left(\frac{-h}{2}D\right)$$

where ΔE is the change in electrostatic energy to form a double kink, h is the kink height, e is the static dielectric constant, D is the Debye screening length, and q is determined by the relative position of the Fermi and dislocation levels. This theory is in qualitative agreement with the observed results, but it predicts a change of magnitude that is six times too small.

The theory of Hirsch (ref. 16) is based on the assumption that energy bands associated with the dislocations are split because of reconstruction. Dangling bonds on kinks give rise to energy levels in the band gap, and they are associated with acceptor and donor energy levels in the gap between the dislocation bands. In this case the number of neutral kinks is unchanged, but the number of charged kinks increases or decreases. The relative change depends on the donor and acceptor levels and on the Fermi level. Dislocation velocity may be enhanced because the total number of kinks is increased and because the mobility of charged kinks may be higher than that of uncharged kinks.

The dislocation velocity (ref. 14) can be described as

$$V = \left(\frac{2\sigma h}{1.73kT}\right) D \exp\left(\frac{-F}{kT}\right)$$

where h is the kink height, F is the energy of kink formation, and D is the kink diffusivity. The term $\exp(-F/kT)$ implies a velocity dependence on the concentration of uncharged kinks. If charged kinks are formed their concentration is given by the expression

$$\frac{C_k}{C_{k0}} = \exp\left(\frac{E_f - E_{ka} - eV}{kT}\right)$$

where E_f is the Fermi level, E_{ka} is the kink acceptor level, and eV is the electrostatic energy of the charged dislocation, including kinks. The new velocity is then given by

$$\frac{V}{V_0} = \exp\left(\frac{E_f - E_{ka} - eV - dW_m}{kT}\right)$$

where dW_m is the difference of dislocation migration energy for charged and uncharged kinks. The velocity may be increased because of the change in kink concentration and because of a possible change in kink migration energy (ref. 16).

The theory of Jones (ref. 25) is similar to that of Hirsch (ref. 16) but assumes that the effect is due to a change in the saddle point configuration energy from reconstruction of kink dangling bonds. Both theories predict a change in the activation energy for migration: Hirsch's model through a change in charged kink migration energy and Jones' model through a change in the saddle point state for charged kinks.

The activation energy for dislocation motion in silicon has been measured as 2.1 eV in intrinsic silicon, 1.4 eV in *n*-type silicon, and 1.6 eV in *p*-type silicon (ref. 20).

The effect of doping on dislocation mobility may lead to significant changes in the DBTT of diamond cubic materials (ref. 24). By indentation of dislocation-free single crystals, the DBTT can be determined by hot microhardness.

Roberts, Pirouz, and Hirsch (ref. 21) studied the effect of doping on DBTT in germanium by using this method. High-purity, single-crystal germanium crystals were indented on the (100) surface with indentor diagonals along the ⟨110⟩ directions. Indentation causes slip on {111} planes and produces prismatic dislocation loops which move out from the indentation site on the prisms formed by the intersection of {111} planes around the indentation. This geometry was suggested in references 13 and 26 and can be seen in figure 4.

Dislocations also move into the material below the indentation with Burgers vectors inclined to the surface. Transmission electron microscope (TEM) examination of dislocation rosettes show only dislocations associated with stacking faults (ref. 27). Dislocations were of the 1/6⟨211⟩ Shockley type (ref. 21). Dislocations with Burgers vectors inclined to the surface may interact to form Lomer-Cottrel locks (ref. 22). In this case the leading partials of two dissociated dislocations may interact to form a sessile dislocation, which can serve to nucleate cracks:

$$\frac{1}{6}[\bar{1}2\bar{1}] + \frac{1}{6}[1\bar{1}2] = \frac{1}{6}[011]$$

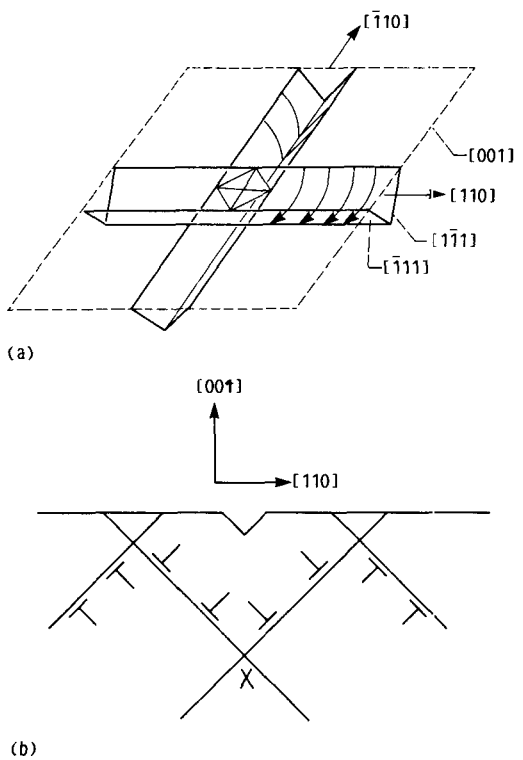

(a) On surface.
(b) Below surface.

Figure 4.—Dislocation configurations on and below surface.

Undissociated dislocations may also react to form Lomer locks:

$$\frac{1}{2}[\bar{1}10] + \frac{1}{2}[0\bar{1}1] = \frac{1}{2}[\bar{1}01]$$

Either of these reactions reduces the energy of the dislocation by reducing the magnitude of the Burgers vector.

Whether or not a crack propagates in a material depends on the mobility of dislocations in that material. Crack propagation depends on a competition between crack-tip decohesive forces and the force necessary for dislocation emission. This is the model of Kelly, Tyson, and Cottrell (ref. 28). If the stress intensity factor for fracture is reached before the critical stress for dislocation emission, the material behaves in a brittle manner. On the other hand, if dislocations are emitted from the crack tip, the local conditions at the crack tip are modified in two ways. First, the dislocations emitted from a crack exert a back stress on the crack, effectively reducing the local stress intensity factor. This is known as crack-tip shielding. Second, the crack tip can also be blunted by dislocation emission. The emission of dislocations of edge character with a Burgers vector normal to the fracture plane will blunt the crack tip, while screw dislocations can jog the crack tip (ref. 29). This effect is known as crack-tip blunting.

Dislocations may also be nucleated by sources in the material near the crack tip. The dislocations, once emitted, are strongly repelled by the crack tip. Three forces act upon the dislocation: (1) the stress field surrounding the crack tip, which repels the dislocation from the crack tip, (2) the image force, which attracts the dislocation to the crack tip, and (3) the edge force, which is a surface tension force due to the creation of new surface at the crack tip (also an attractive force).

The interaction of these three forces creates a position of unstable equilibrium. Once this position is crossed, the dislocation is repelled strongly and moves away from the crack tip until it encounters some obstacle (ref. 30). The TEM observations by Ohr (ref. 31) show that dislocations move rapidly away from the crack tip, leaving a small dislocation-free zone (DFZ) around the tip. Ohr suggests that this DFZ is a result of the short range of the image force attracting the dislocations to the crack tip. As a result, the dislocations always experience a repulsive force. Li (ref. 32) suggests that this is because the dislocations around the crack retract into it after unloading.

Dislocation from sources near the tip may also play a role as they are attracted or repelled from the crack tip. Dislocations repelled by the crack tip come to rest in dense tangles some distance away, forming a plastic zone. This plastic zone shields the crack tip from the applied stress. This process, however, may not continue indefinitely. Dislocations may interact to produce pileups and wedge-shaped defects dependent on slip geometry in the material (ref. 33).

The stress intensity factor K_e required for dislocation emission is derived in reference 29:

$$K_e = (2Gb\sigma_f)^{1/2}$$

where G is the shear modulus, σ_f is the yield stress, and b is the magnitude of the Burgers vector. It is shown that the stress required for dislocation emission is proportional to the square root of the flow stress. This value has been measured by Michot and George (ref. 34) to be 0.16 to 0.24 MPa/m^2 for float-zone silicon and 0.3 to 0.4 MPa/m^2 for CZ silicon in the temperature range 700 to 850 °C.

Ashby and Embury (ref. 35) have reported that the dislocation density of a material may determine if it behaves in a ductile or brittle manner. In body-centered cubic (bcc) materials, increases in dislocation density provided by plastic working have given rise to decreases in the DBTT. The explanation is based on the access of the crack tip to mobile dislocations. If the crack tip has access to dislocations, these may move and multiply, and thus inhibit crack growth. However, if it does not, the crack can propagate at low K_c. A simple model was proposed in which DBTT is directly related to dislocation density (ref. 35). The transition temperature falls slowly with increasing dislocation density until the latter is high enough that dislocation interactions cause significant increases in the flow stress. This model also predicts that increases in dislocation velocity will reduce the DBTT.

Dislocation emission from crack tips is a necessary but not sufficient condition for plasticity (unpublished work by M. Brede and P. Haasen). Dislocations must also be able to move away from the tip rapidly enough to avoid the creation of a brittle condition.

Ductile-Brittle Transition in Silicon

A significant amount of investigation on the DBTT in silicon has been performed. Table I is a summary of the DBTT values given in references 34 and 36 to 39. The DBTT varies from about 550 to 1050 °C and is rate dependent. St. John (ref. 36) first studied the ductile-brittle transition in silicon. He reports that the DBTT is strongly rate dependent and varies from 700 to 950 °C, increasing with increasing strain rate. The DBTT occurs over a very narrow temperature range, as narrow as 5°. The load for fracture increases with increasing strain rate.

Hirsch, Roberts, and Samuels (ref. 37) investigated the ductile-brittle transition in silicon and found lower transition temperatures but a similarly sharp transition and dependence on strain rate. They suggest that the DBTT is controlled by

TABLE I.—DUCTILE-BRITTLE TRANSITIONS IN SILICON

Author	Reference	Strain rate, μm/min	Ductile-brittle transition temperature, °C	Comments
G. Michot and A. George	34	5 50 500	705 805 942	Float zone
C. St. John	36	5 10 50 100 500	700 725 800 850 925	*p*-Type
P.B. Hirsch et al.	37	Unknown	600 550	Float zone
R. Behrensmeier et al.	38	50 50 50	680 685 705	Oxygen dopant
W.D. Sylvestrowicz	39	1400	1080	Float zone or Czochralski
M.Brede and P. Haasen	(a)	5 10 25 50 100 250 500	671 702 712 752 802 852 877	Float zone Czochralski Czochralski Czochralski Czochralski Float zone Float zone
J. Schauer and P. Pirouz	(b)	5	691	Float zone

[a]Unpublished work.
[b]The Effects of Mode I and Mixed Mode Loading on the Brittle Ductile Transition in Single Crystal Silicon, MSc. Thesis, Case Western Reserve University, Cleveland, OH, 1987.

the activation energy for dislocation motion. The sharpness of the transition is due to the difficulty of forming operating sources in pure and dislocation-free materials like silicon. The K for activating sources is 95 percent of K_{1c}, and the transition is very sharp. These sources are formed when dislocations are attracted to the crack tip and by cross slip become sources for dislocation generation. The differences in DBTT in references 36 and 37 are attributed to a much lower dislocation density in the experiments of reference 36. In reference 37, many dislocations were produced by an indentation process. Silicon provides an extreme example of the effect of dislocation density described in reference 35. However, when dislocation sources already exist at or near the crack tip and can be activated by low values of K, the blunting of crack tips is not dependent on a nucleation phenomenon, but only on the rate at which dislocations move away from the crack tip. In this case, the fracture transition is not sharp and is accompanied by increasing dislocation activity around the crack tip.

Behrensmeier et al. (ref. 38) studied the DBTT in oxygen-doped silicon and showed that the DBTT can be varied by appropriate heat treatment. A treatment that caused oxygen precipitates to form extrinsic stacking faults caused a lower DBTT, since these precipitates serve as sources for dislocation production and multiplication. Heat treatments that resulted in amorphous platelets of silicon dioxide also resulted in higher DBTT because of dislocation pinning. Changes of up to 25 °C in DBTT were produced by appropriate heat treatments.

The DBTT was measured for both float-zone and CZ silicon in reference 34. By using strain rates of 1.6 to 500 μm/min, DBTT values of 698 to 942 °C were produced. The DBTT increased with increasing strain rate. CZ silicon always displayed a higher DBTT than float-zone silicon in this work. Since measurements show that the velocity of dislocations in silicon is the same for CZ and float-zone for stresses above 5 MPa, the results may be due to dislocation locking in CZ crystals (ref. 34).

Sylwestrowicz (ref. 39) deformed silicon single crystals in tension at high strain rates and temperatures. He reports a DBTT value of 1080 °C at a strain rate of 1400 μm/min.

An unpublished study of the DBTT in silicon over a wide temperature range by M. Brede and P. Haasen reports values of 671 to 877 °C for strain rates of 5 to 500 μm/min. The DBTT increased with strain rate, as in reference 34.

Puttick (ref. 40) compared the DBTT expected in various types of mechanical testing. He suggests that a DBTT occurs when a characteristic length, that of an inhomogeneous stress field, reaches a critical value. This value is proportional to a material factor $(K_{1c}/Y)^2$, where Y is the yield stress in a uniaxial test.

By calculating a constant of proportionality for several tests, it can be shown that the DBTT obtained is a strong function of the type of test (ref. 4). The Hertzian indentation test, with its very short range tensile field, produces the lowest DBTT, followed by elastic-plastic indentation, bend testing, and notch tensile testing, which produces the highest DBTT.

Experiment

High-purity, float-zone, dislocation-free, single crystal silicon ingots were obtained from Wacker Chemitronic. The ingots were approximately 4 in. in diameter and were obtained with heavy boron doping (p-type), with phosphorus doping (n-type), and without intentional doping (intrinsic). All crystals were grown along the ⟨111⟩ orientation. The p-type material was boron-doped to a concentration of $4.5\times10^{17}/cm^3$ and had a resistivity of 7.5×10^{-2} Ω cm. The n-type material was phosphorus-doped to a concentration of $6\times10^{18}/cm^3$ and had a resistivity of 8.4×10^{-3} Ω cm. Intrinsic material was n-type, with a carrier concentration of $2\times10^{12}/cm^3$, and had a resistivity of 2000 Ω cm. Each material was tested for resistivity by using a four-point probe technique, and all agreed closely with the documentation provided.

Sections of each sample were diamond sawed for mounting on a goniometer and oriented by using the Laue method. The specimens were again diamond sawed to provide a (100) face, and the ⟨110⟩ directions were scribed on this surface by reference to the Laue pattern. Estimated accuracy of this technique was about ±1°. The samples were cut into 5- by 5- by 10-mm specimens with edges parallel to the ⟨110⟩ directions. Each specimen was mounted with hot melt cement, mechanically polished on 600-grit silicon carbide paper, on 3-μm diamond, 1-μm diamond, and 0.3-μm alumina grits, and then finished on colloidal silica (SYTON) in a vibratory polisher.

Specimens were indented in a Nikon QM hot microhardness machine. Both the specimen and indenter were heated and maintained at a vacuum in the 10^{-5} range. Indents were initially made at 100-g load by using a Vickers indenter with the diagonals along the ⟨110⟩ directions. Dwell time for the indenter was 15 sec. Indentations were made at 50 °C increments from 850 to 350 °C. Additional measurements were made at 200, 300, and 500 g in some cases.

Measurements of crack lengths and the temperature at which they began to form were noted. An additional series of indents was made at 100-g and 10 °C increments to more closely measure the ductile-brittle transition. Measurements of hot microhardness were also made in some cases. At least six widely spaced indents were made and measured in all cases.

After the specimen was removed from the machine it was etched in a mixture of 4 parts 40 percent hydrofluoric acid to 1 part 0.25 molar potassium dicromate for about 30 sec. This mixture is a dislocation etch and reveals dislocations generated by indentation. Dislocations were confined to the ⟨110⟩ directions. Measurements were made of the dislocation rosette diameters produced.

Another series of specimens was indented at 100, 300, and 500 g and sectioned 500 μm below the surface with a diamond saw. These specimens were mounted face down on a glass plate with clear nail polish and backthinned to 150 μm. Each sample was then carefully thinned by mechanical polishing to 100, 75, 50, and 25 μm. These samples were polished only through 0.3 μm alumina because of their delicate nature. The sample was etched by using the dislocation etchant at each stage, and the size and shape of the plastic zone and dislocation rosettes were measured.

All measurements are presented in tabular and graphical form in the following section.

Results and Discussion

Hardness of Silicon

Figure 5 shows the indentation diagonal measured in *p*-type, *n*-type, and intrinsic silicon at 300-g load. The *n*-type silicon displayed the greatest indentation diagonal, followed by *p*-type, and then intrinsic. This behavior persisted from 700 to 600 °C. No significant differences in indentation diagonal were apparent below 600 °C. Diagonal lengths for all loads and dopings are presented in table II.

Figure 6 shows the hardness of doped and intrinsic silicon as a function of temperature at 100- and 300-g loads. Values used in constructing these graphs are found in table III.

TABLE II.—INDENTATION DIAGONALS IN *n*-TYPE, *p*-TYPE, AND INTRINSIC SILICON

[Mean and standard deviation are denoted by μ and σ, respectively.]

Temperature, °C	Load, g	Indentation diagonal, μm					
		n-Type		*p*-Type		Intrinsic	
		μ	σ	μ	σ	μ	σ
700	500	----	---	80.6	1.8	----	---
	300	69.5	1.6	63.3	1.8	59.0	0.7
	100	37.5	.8	35.5	.8	32.4	.6
600	500	----	---	57.0	1.2	----	---
	300	45.7	1.8	43.4	.8	41.1	0.9
	100	26.4	.8	25.0	.6	23.7	.7
500	500	----	---	42.5	2.1	----	---
	300	33.4	1.2	32.1	1.1	31.6	1.5
	100	18.2	.5	18.0	.6	18.1	.8
400	500	----	---	38.2	3.5	----	---
	300	27.9	1.1	27.0	2.5	26.9	0.8
	100	14.9	.5	14.6	.7	15.5	.4
300	500	----	---	31.8	1.6	----	---
	300	22.9	0.8	26.1	1.5	24.3	0.9
	100	13.2	.7	15.0	1.0	13.2	.4
200	500	----	---	35.1	2.7	----	---
	300	22.8	1.3	20.8	2.0	22.7	0.8
	100	11.4	.5	10.0	.5	12.4	.6

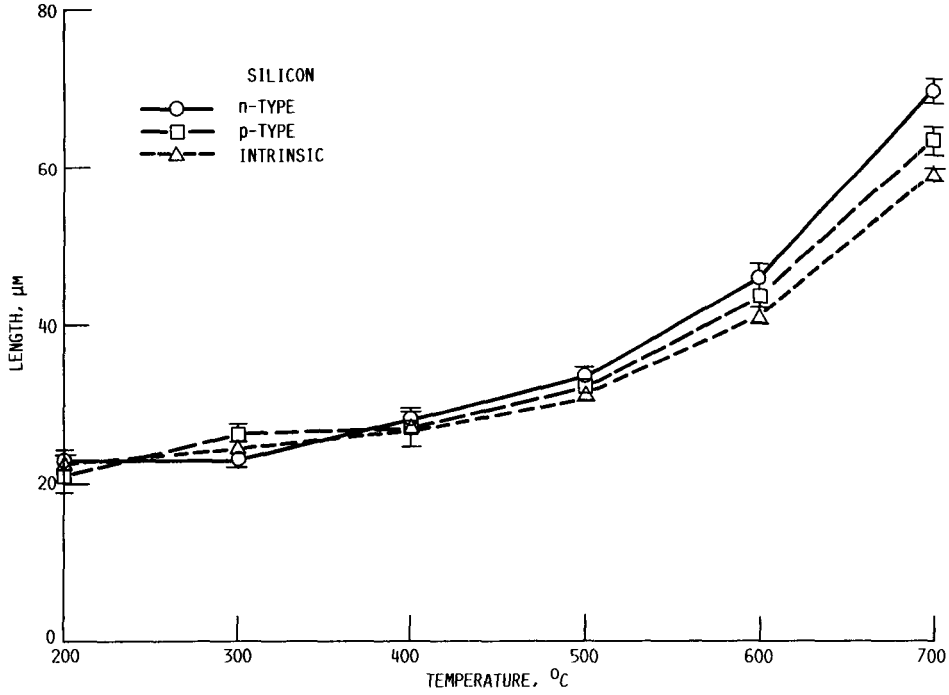

Figure 5.—Effect of doping on indentation diagonal at 300-g load.

Hardness values ranged from about 1 GPa at 700 °C to about 15 GPa at 200 °C. This is in good agreement with the results given in references 9 and 10. Both 100- and 300-g loads gave similar results, but the 300-g load hardnesses were a little lower, especially at low temperatures. At 200 °C any trends are obscured by scatter in the data. Figure 7 shows hardness as a function of load and temperature for *p*-type silicon. All loads produced equivalent hardness at high temperatures, but at intermediate temperatures, lower loads produced higher hardnesses. At low temperatures, scatter in the data obscured

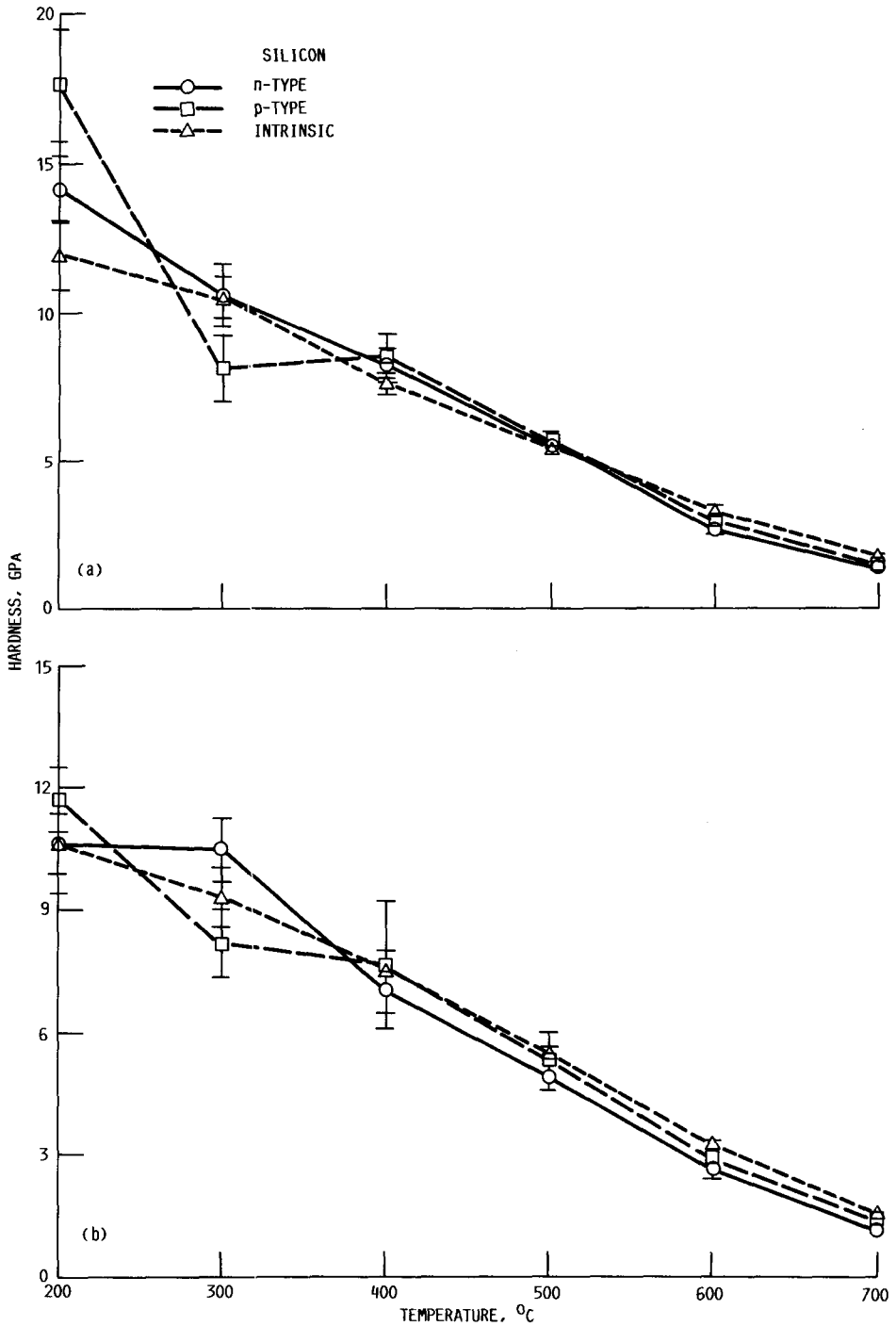

(a) 100-g load.
(b) 300-g load.

Figure 6.—Effect of doping on hardness.

TABLE III.—HARDNES OF *n*-TYPE, *p*-TYPE, AND INTRINSIC SILICON

[Mean and standard deviation are denoted by μ and σ, respectively.]

Temperature, °C	Load, g	Hardness, GPa					
		n-Type		*p*-Type		Intrinsic	
		μ	σ	μ	σ	μ	σ
700	500	-----	----	1.40	0.07	-----	----
	300	1.13	0.05	1.36	.08	1.56	0.04
	100	1.29	.06	1.44	.07	1.73	.06
600	500	-----	----	2.80	0.12	-----	----
	300	2.63	0.23	2.89	.11	3.23	0.12
	100	2.62	.15	2.92	.13	3.24	.23
500	500	-----	----	5.06	0.58	-----	----
	300	4.90	0.33	5.31	.36	5.49	0.53
	100	5.48	.31	5.62	.38	5.58	.43
400	500	-----	----	6.91	1.25	-----	----
	300	7.02	0.54	7.65	1.56	7.55	0.47
	100	8.22	.58	8.52	.74	7.60	.39
300	500	-----	----	8.45	0.38	-----	----
	300	10.47	0.78	8.18	.84	9.31	0.72
	100	10.55	1.02	8.12	1.10	10.49	.70
200	500	-----	----	7.47	1.10	-----	----
	300	10.59	1.21	11.68	.80	10.65	0.74
	100	14.08	1.12	17.56	1.89	11.89	1.14

any trends. Scatter in the low temperature data can make reliable hardness values difficult to obtain.

The effect of hardness on load is a manifestation of recovery of the indents at low loads. Values at low temperatures may also be somewhat more erratic, since heavy fracturing of the surface made accurate measurements difficult. The very small size of low temperature indents also complicated the diagonal measurements. Figure 8 shows micrographs of indents made above and below the DBTT, at 100-g load.

The type of doping also had an effect on the hardness of silicon. In the 100-g tests no significant difference was found with doping. In the 300-g tests *n*-type and *p*-type doping produced slightly lower hardnesses than in intrinsic samples above 600 °C. The effect of doping is easier to see in the diagonal length measurements of figure 5.

Cracking and Ductile-Brittle Transition Temperature

During hardness testing it was found that the material was ductile above a certain temperature, and that below this temperature, indents were always surrounded by cracking. Figure 9 is a plot of the crack lengths measured around the indents as a function of temperature; crack length data are found in table IV. The curves of figure 9 show a ductile-brittle transition near 700 °C for intrinsic and *p*-type silicon and at about 650 °C for *n*-type silicon. More careful experiments

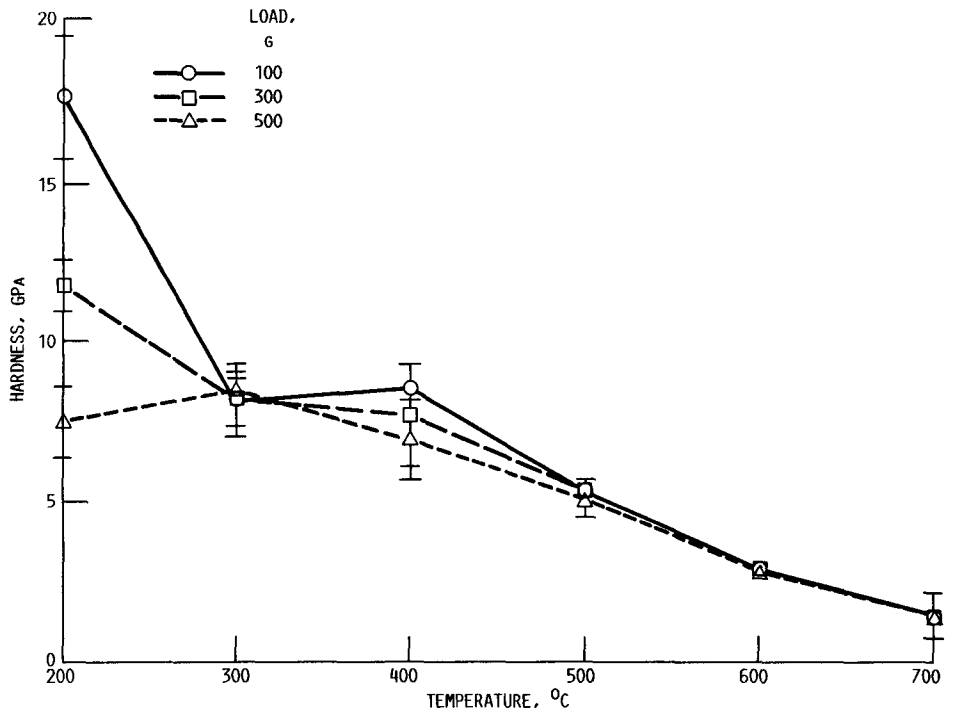

Figure 7.—Effect of load on hardness for *p*-type silicon.

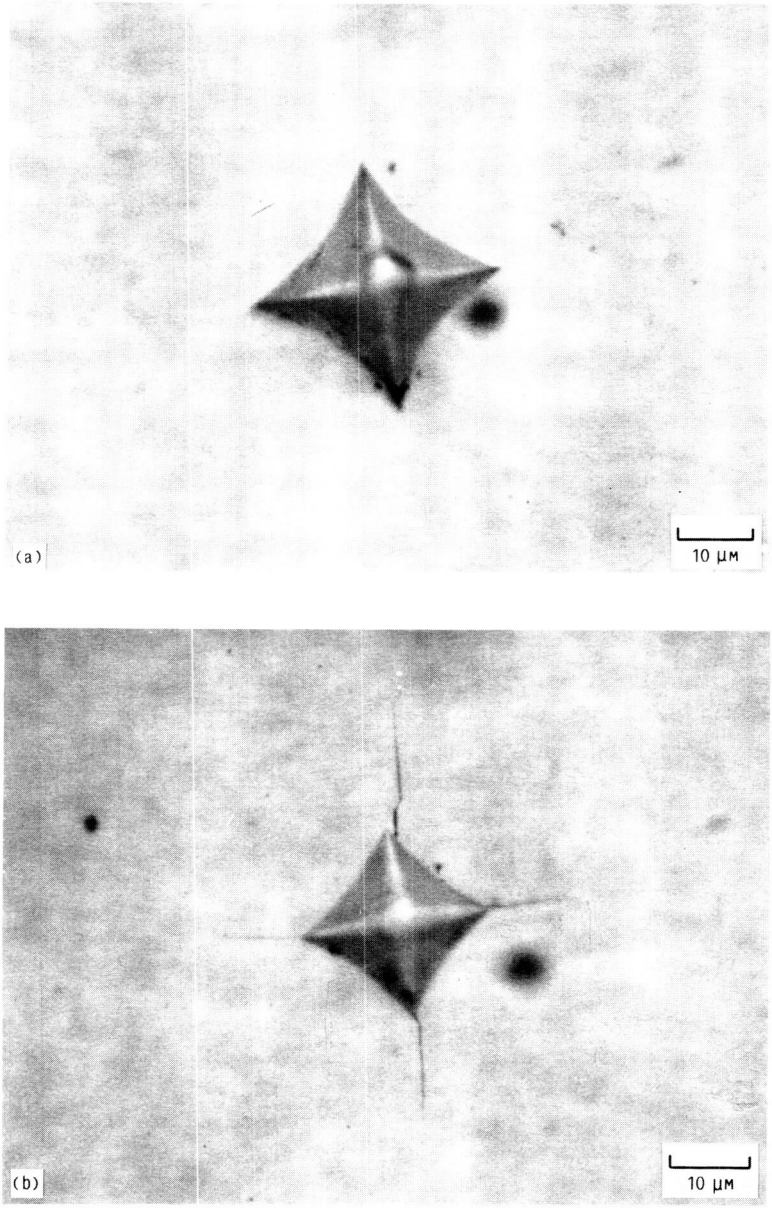

(a) Above DBTT (700 °C).
(b) Below DBTT (600 °C).

Figure 8.—Indents above and below ductile-brittle transition temperature (DBTT) at 100-g load.

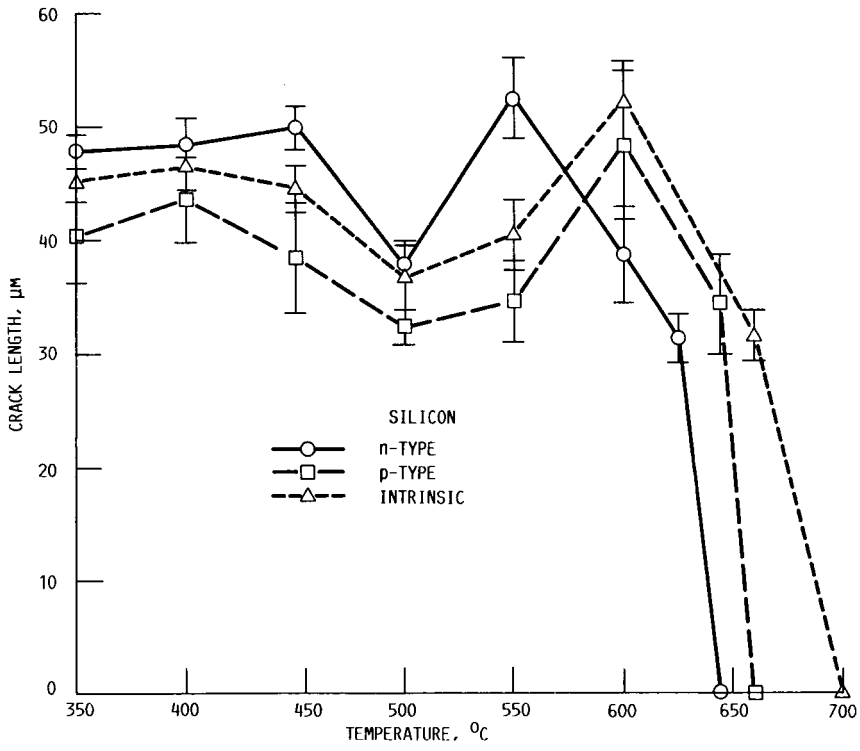

Figure 9.—Effect of doping on crack length and ductile-brittle transition temperature (DBTT) at 100-g load.

TABLE IV.—CRACK LENGTH DATA FOR *n*-TYPE, *p*-TYPE, AND INTRINSIC SILICON

[Mean and standard deviation are denoted by μ and σ, respectively.]

Temperature, °C	Crack length, μm							
	n-Type[a]		*p*-Type[a]		Intrinsic[a]		Intrinsic[b]	
	μ	σ	μ	σ	μ	σ	μ	σ
750	0	0	0	0	0	0	0	0
700	0	0	0	0	0	0	0	0
650	0	0	34.2	4.3	31.6	2.1	59.9	9.3
600	38.6	4.2	48.3	6.6	52.2	3.5	81.8	2.8
550	52.5	3.6	34.6	3.6	40.4	3.1	54.2	5.6
500	37.8	2.1	32.3	1.5	36.6	2.9	53.9	5.8
450	49.9	1.9	38.4	4.9	44.5	2.1	62.4	2.2
400	48.3	2.4	43.5	3.8	46.4	2.0	66.1	4.1
350	47.8	1.5	40.3	4.1	45.3	1.9	66.9	3.5

[a]100-g load.
[b]200-g load.

showed DBTT's as follows: intrinsic, 660 °C; *p*-type, 645 °C; and *n*-type, 625 °C. The values are lower than those given in reference 36 but in line with those of reference 37. These discrepancies may arise from the use of different test methods for determining the DBTT. In reference 36, the samples were dislocation free, and any dislocations must have been generated from or near the crack tip. In the work reported in reference 37, microhardness indentations were used to generate sharp cracks, and thus the crack tip had access to some dislocations. In the experiments here, microhardness indentations were used to determine DBTT, and thus many dislocations were near the crack tip. As a result, the DBTT values are more in line with those of reference 37.

Figure 10, a comparison of crack lengths with 100- and 200-g load in intrinsic silicon shows that the DBTT is not changed. In figures 9 and 10 the length of the cracks shows a maximum below the DBTT.

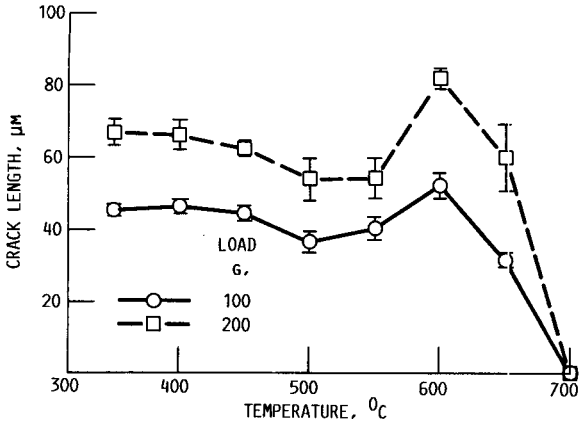

Figure 10.—Effect of load on crack length for intrinsic silicon.

Figure 11 shows the effect of temperature and doping on apparent fracture toughness; data are presented in table V. The apparent fracture toughness, calculated from crack lengths, at 100-g load (fig. 11(a)) varies from a low of about 0.90 MPa $m^{1/2}$ at 400 °C to about 3 MPa $m^{1/2}$ near the DBTT. Figure 11(b) is fracture toughness calculated from data taken at 300-g load. Fracture toughness values range from about 0.90 MPa $m^{1/2}$ to a high of about 1.2 MPa $m^{1/2}$ over the temperature range studied. These values are slightly higher than the room-temperature values given in references 10 and 12. Doping does not seem to significantly affect the fracture toughness of silicon.

The presence of a DBTT is expected in materials of limited dislocation mobility. Body-centered cubic (bcc) metals and diamond cubic semiconductors are examples of such materials. This effect is expected to be observed at about 60 percent of

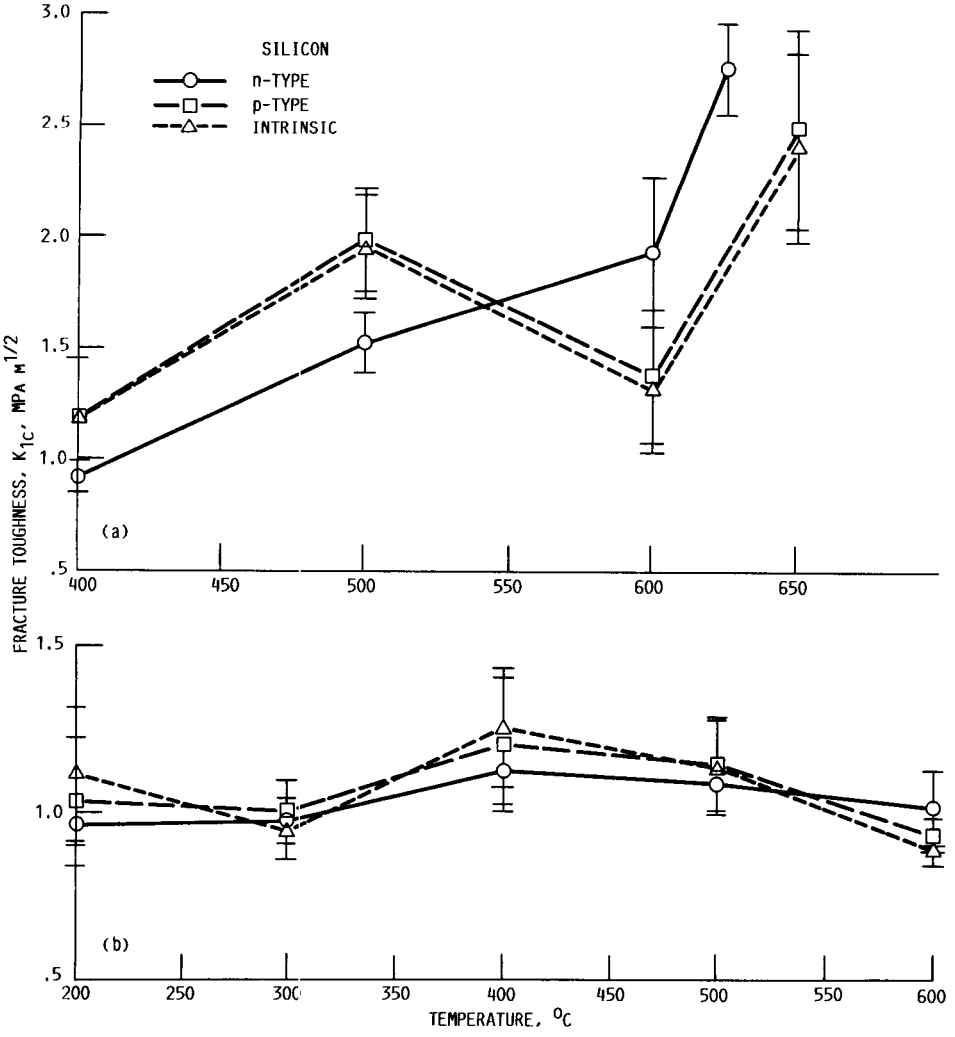

(a) 100-g load.
(b) 300-g load.

Figure 11.—Effect of doping on fracture toughness.

TABLE V.—FRACTURE TOUGHNESS DATA FOR *n*-TYPE, *p*-TYPE, AND INTRINSIC SILICON

[Mean and standard deviation are denoted by μ and σ, respectively.]

Temperature, °C	Fracture toughness, MPA $m^{1/2}$					
	n-Type		*p*-Type		Intrinsic	
	μ	σ	μ	σ	μ	σ
300-g Load						
700	----	----	----	----	----	----
600	1.01	0.11	0.93	0.05	0.89	0.05
500	1.08	.08	1.14	.14	1.13	.14
400	1.12	.10	1.20	.20	1.25	.18
300	.97	.07	1.00	.09	.94	.08
200	.96	.06	1.03	.19	1.11	.20
100-g Load						
700	----	----	----	----	----	----
650	----	----	2.48	0.45	2.40	0.43
625	2.76	0.20	----	----	----	----
600	1.92	.34	1.37	.30	1.31	.28
500	1.52	.13	1.98	.23	1.95	.23
400	.92	.07	1.19	.25	1.20	.25

their absolute melting temperature (ref. 24). This would be about 750 °C for silicon but could be affected by electrically active impurities, as observed here.

Cracking around the indents is expected to be associated with the formation of Lomer or Lomer-Cottrell locks. Dislocations with their Burgers vectors inclined to the surface react at the intersection of {111} planes in the plastic zone below the indent (ref. 22). These intersections result in the formation of sessile dislocations with a Burgers vector lying outside the glide plane. These dislocations serve as crack nuclei. Crack growth will occur when the mobility of dislocations surrounding these nuclei is no longer high enough to blunt the cracks formed. At this time stresses formed by loading can result in the growth of a crack nucleus into a median crack, or upon unloading, the residual stress can nucleate shallow lateral cracks. Temperature and doping affect the dislocation mobility in these materials. As temperature falls so does dislocation mobility. Doping can increase the dislocation mobility in silicon at a given temperature by increasing the actual kink concentration above the equilibrium kink concentration.

The effect of doping on the DBTT is apparent in the results. Intrinsic silicon displays the highest DBTT, followed by *p*-type, and then *n*-type materials. It is known that *n*-type doping has the greatest effect on dislocation mobility. Higher dislocation mobility will make it increasingly difficult for cracks to propagate from the Lomer or Lomer-Cottrell locks, because it will increase the effectiveness of crack blunting mechanisms. Thus *n*-type silicon displays the lowest DBTT, followed by *p*-type material, in which there is a smaller effect on dislocation velocity, and then by intrinsic silicon, which has the highest DBTT.

The effect of load on crack length is roughly as expected according to the model described in reference 8: a doubling of the load produces a 50-percent increase in crack length. The peak in the crack length curve as a function of temperature is a result of the large size of the plastic zone near the DBTT. At these temperatures any crack nucleated during loading can grow on as the surface goes into tension on unloading. The stress is generated as a result of plastic deformation during indentation. On unloading, the mismatch between the elasticly and plasticly deformed regions causes these stresses to develop. These stresses can also nucleate shallow lateral cracks on unloading. The peak in the crack length curve is a result of the large amount of plastic deformation near these temperatures. Above these temperatures fracture toughness begins to increase, and the crack length falls off. Below the maximum the amount of plastic deformation is small, and thus the increase in crack length on unloading is reduced. A combination of these effects leads to a maximum in the crack length curve.

The apparent fracture toughness of silicon varies from about 0.90 MPa $m^{1/2}$ to about 3.0 MPa $m^{1/2}$ over the temperature range 200 to 600 °C. In the 300-g data, fracture toughness is fairly constant with temperature. In the 100-g data, which more closely approach the DBTT, a strong increase in fracture toughness occurs near the DBTT. An increase in fracture toughness with temperature, especially near the DBTT, would be expected as dislocation mobility and plasticity play an increasingly important role. The values presented here were calculated by using the room-temperature values of Young's modulus and the high-temperature values of hardness obtained in this work. Modulus does vary to some extent with temperature; this may have affected the results to some degree, obscuring an increase in K_{1c} with temperature in the 300-g data.

Fracture toughness of silicon does not seem to be greatly affected by doping. Values for intrinsic silicon were slightly lower than for *n*-type or *p*-type material, especially in the lower temperature range. However, no clear trends emerge, and any variations are obscured in data scatter. This behavior is not surprising since any effect below the DBTT is associated with increasingly lower amounts of dislocation activity. The main effect of doping is in lowering the temperature at which the ductile-brittle transition occurs.

Dislocation Rosettes and Plastic Zone Size

After etching, arrays of dislocations could be observed emanating from the plastic zone surrounding the indent along the ⟨110⟩ directions. It should be recalled that the indent diagonals were aligned along the ⟨110⟩ directions for all the tests. These dislocation rosettes measured for each material are presented in table VI and in figure 12. Micrographs of rosettes are shown in figure 13. Rosettes were largest at high temperatures. In no cases were dislocation rosettes observed on the surface below 500 °C. Lengths varied from zero at 500 °C to 500 μm in diameter at 850 °C. The rosette lengths

TABLE VI.—DISLOCATION ROSETTE DIAMETERS FOR *n*-TYPE, *p*-TYPE, AND INTRINSIC SILICON

[Mean and standard deviation are denoted by μ and σ, respectively.]

Temperature, °C	Rosette diameter, μm							
	n-Type[a]		*p*-Type[a]		Intrinsic[a]		Intrinsic[b]	
	μ	σ	μ	σ	μ	σ	μ	σ
850	248.5	14.8	489.7	11.3	447.5	11.6	576.4	26.2
800	237.0	8.5	460.9	7.8	416.8	10.3	475.7	25.4
750	217.7	11.3	388.7	8.4	365.7	7.5	400.4	18.4
700	180.9	14.0	314.3	11.0	289.0	9.5	331.4	9.8
650	120.9	5.1	198.1	8.3	201.7	5.7	225.9	14.8
600	98.1	5.3	127.3	8.8	128.4	5.6	148.7	6.0
550	66.0	2.7	69.7	5.3	84.0	2.1	93.2	4.5
500	0	0	0	0	0	0	0	0

[a]100-g load.
[b]200-g load.

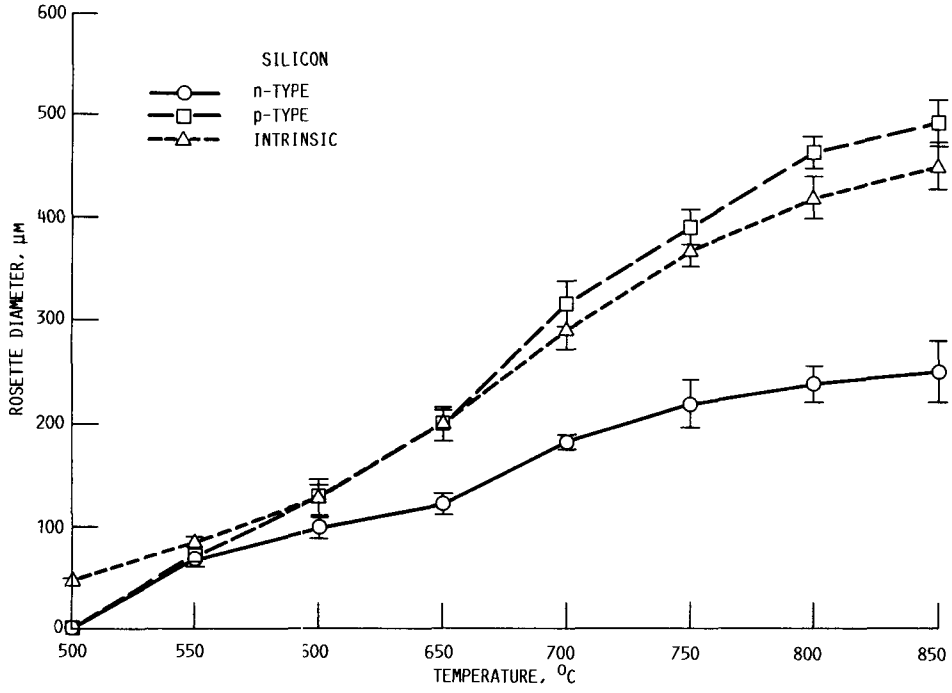

Figure 12.—Effect of doping on rosette length at 100-g load.

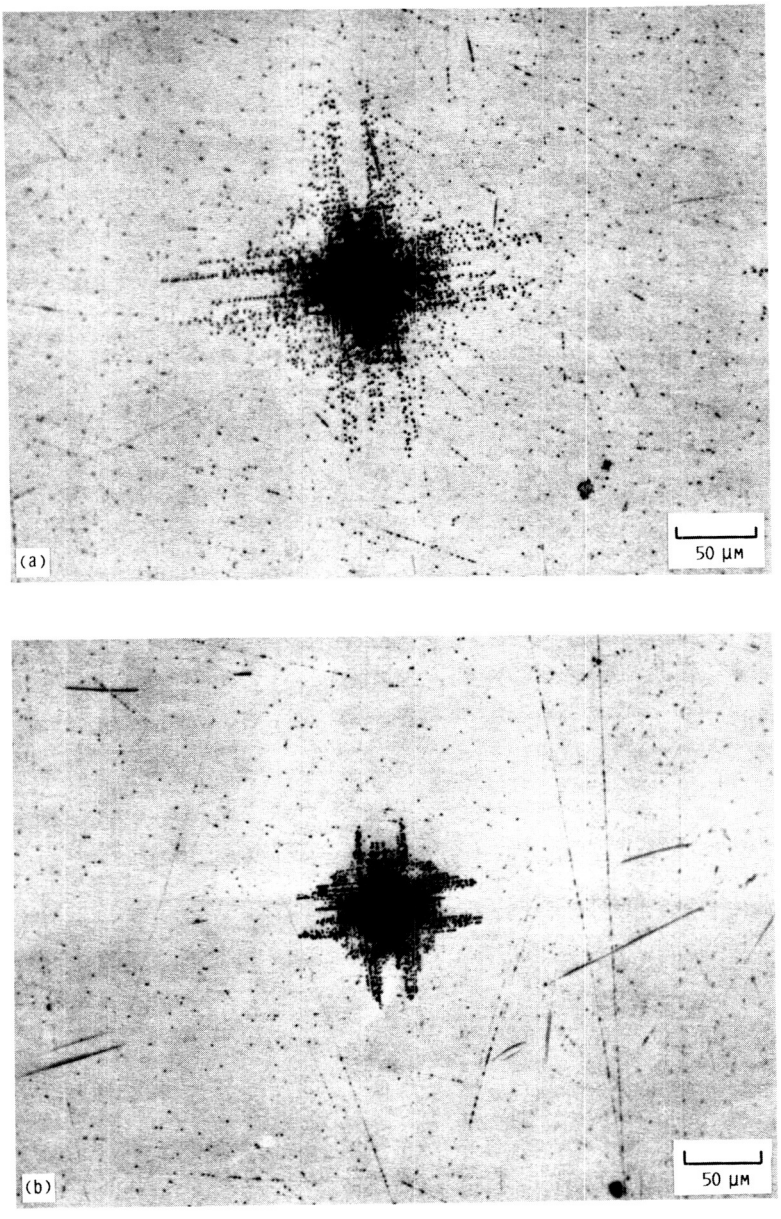

(a) At 700 °C.
(b) At 600 °C.

Figure 13.—Dislocation rosettes on surface revealed by etching.

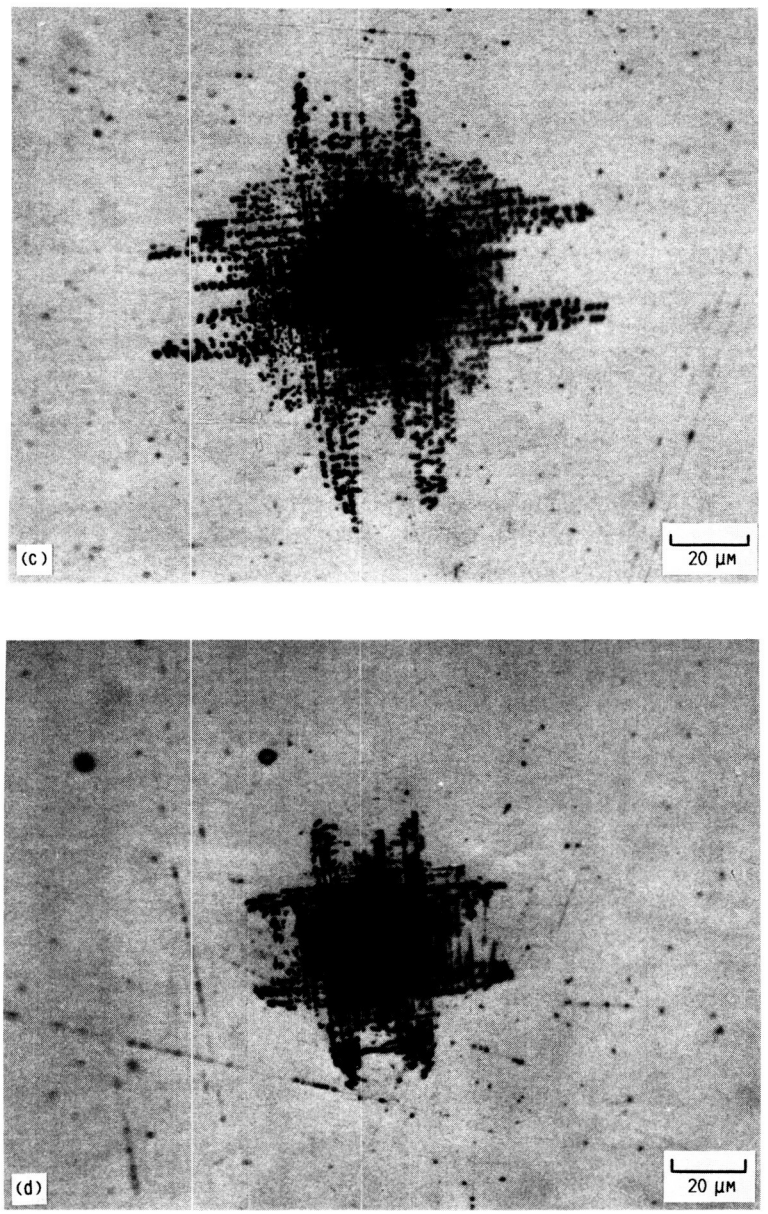

(c) Part (b) at greater magnification.
(d) At 550 °C.

Figure 13.—Concluded.

were largest for *p*-type silicon followed by intrinsic silicon and, puzzlingly, lowest for *n*-type silicon. The *n*-type rosette measurements were repeated many times and always produced the shortest rosette lengths. Rosettes were largest at high temperatures where dislocation mobility was highest. Although both *n*- and *p*-type doping should increase rosette diameters, only *p*-type doping did. It is not clear why *n*-type doping, which is expected to have the greatest effect in increasing dislocation mobility and does have the greatest effect in reducing the DBTT, would not have a similar effect on rosette dislocation size. One possibility may be that the *n*-type material etched less easily than the intrinsic and *p*-type materials, and thus the full size of the rosettes was not revealed. Difficulty in etching *n*-type silicon is reported in reference 11. Figure 14 shows the effect of load on rosette length in intrinsic silicon; doubling the load produced only a modest increase in rosette length.

A plot of the natural logarithm of rosette diameter as a function of the inverse temperature was constructed and the slopes calculated. Analysis of the slopes provided activation energy values of 0.278 eV for *p*-type, 0.196 eV for *n*-type, and 0.265 eV for intrinsic silicon, all measured from 700 to 850 °C. These values are inconsistent with known values for activation energy of dislocation motion. Microhardness is not a useful tool for measuring these energies, possibly because of the interaction of the many dislocations generated by indentation.

Dislocations induced around the indents are of two types. Some dislocations are produced by displacement of material below the indenter, forming the plastic zone. Other dislocations extend out into the elastic zone, forming rosettes. Dislocations underneath the indent, which form the plastic zone, glide on {111} planes with Burgers vectors inclined to the surface. Rosette dislocations move on the {111} planes with Burgers vectors parallel to the surface. Dislocations with Burgers vectors inclined to the surface are generated at the surface by displacement of material into the crystal, while those with Burgers vectors parallel to the surface move out from the indent along the ⟨110⟩ directions (ref. 22). Figure 5 shown the crystallography of the dislocation configurations. Dislocations on {111} planes with Burgers vectors parallel to the surface are separated by 90°, and dislocations with Burgers

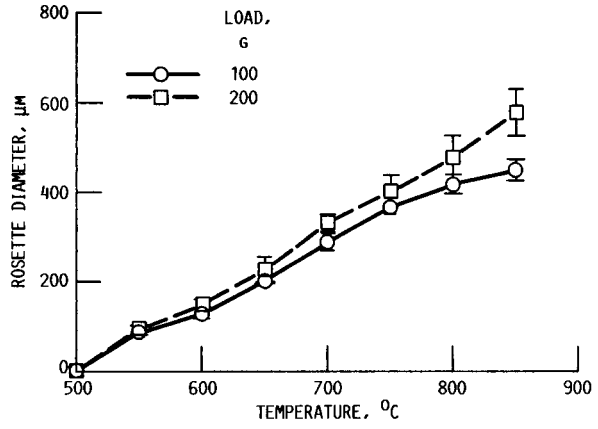

Figure 14.—Effect of load on rosette length for intrinsic silicon.

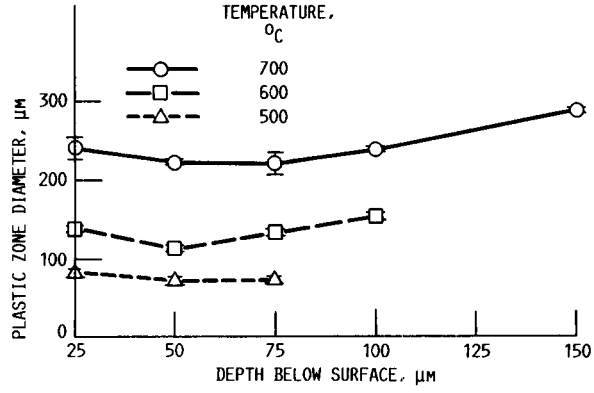

Figure 15.—Plastic zone diameter as function of depth below surface for *p*-type silicon.

TABLE VII.—PLASTIC ZONE DIAMETERS

[Mean and standard deviation are denoted by μ and σ, respectively.]

Temperature, °C	Load, g	Depth below surface, μm									
		150		100		75		50		25	
		Plastic zone diameter, μm									
		μ	σ	μ	σ	μ	σ	μ	σ	μ	σ
700	500	337.5	17.7	330.0	14.1	320.0	3.5	305.0	7.1	320.0	14.1
	300	287.5	3.5	237.5	3.5	220.0	14.1	222.0	3.5	240.0	14.1
	100	0	0	142.7	2.5	112.5	3.5	100.0	7.0	132.5	10.6
600	500	0	0	176.7	11.6	160.0	7.1	152.0	3.5	167.5	3.5
	300	0	0	152.5	3.5	132.5	3.5	112.5	3.5	137.5	3.5
	100	0	0	0	0	0	0	62.5	3.5	72.5	3.5
500	500	0	0	0	0	156.7	5.8	107.5	3.5	97.5	3.5
	300	0	0	0	0	72.5	3.5	71.5	5.0	82.5	3.5
	100	0	0	0	0	0	0	0	0	0	0

vectors inclined to the surface glide on {111} planes inclined to the surface by 54.75°.

Rosettes produced by etching the surface provided one measure of dislocation activity around the indenter; backthinning indented samples provided another. Figure 15 shows the depth below which no dislocation etch pits were produced by etching the sample. The size of the plastic zone as a function of temperature, load, and depth below the surface is given in table VII. Slip below the indenter produced dislocation activity from a depth of >150 μm at 700 ° C and 500-g load to a depth of <25 μm at 500 °C and 100-g load. Rosette diameters varied from zero at a certain depth below the surface to a maximum near the surface, near that value observed on the surface. Figure 16 shows the diameter of the rosettes below the surface as a function of depth and temperature. Figure 17 shows the patterns produced by etching the backthinned samples. Data are presented in table VIII.

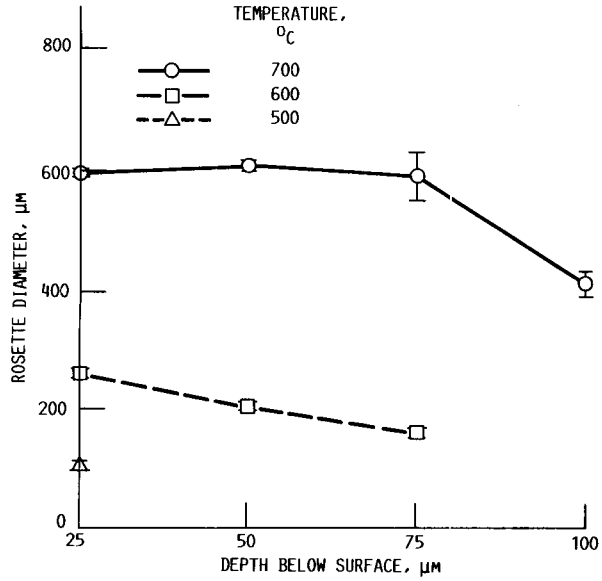

Figure 16.—Rosette diameter below surface for *p*-type silicon at 300-g load.

Figure 17(a) shows the type of pattern associated with shallow depths below the surface. Rosette dislocations are visible, and their diameter is comparable to the diameter observed on the surface. Rosette dislocations were present to a depth of 75 to 100 μm at 700 °C, to a depth of 50 to 75 μm at 600 °C, and only to a depth of 25 to 50 μm at 500 °C, at 300-g load. At higher loads rosettes were present to a greater depth, and at lower loads to a lesser depth. Figure 17(b) shows the pattern associated with somewhat greater depth (75 μm in this case) where rosette dislocations are no longer present. The plastic zone, however, is still heavily populated with etch pits. The size of the plastic zone increased slowly with depth and is independent of whether of not rosette dislocations were present. Data on plastic zone diameter are presented in table VII. Increasing the load 3 or 5 times increased the diameter of the plastic zone by factors of approximately 2 and 2.5 times, respectively. This is in fairly good agreement with the effect of increasing load on indentation diagonal, a P/l^2 relationship. Plastic zone size should be linearly related to indentation diagonal. Figure 17(c) shows the etch pit pattern far below the surface near where the pattern will disappear. The outside of the plastic zone is still outlined by etch pits, and some internal structure is visible. Figures 17(d) and (e) show more detailed views of structure in the plastic zone. It appears that dislocations formed by the opposite corners of the indents are annihilating each other as they interact on intersecting {111} planes.

TABLE VIII.—BACKTHINNING ROSETTE DIAMETERS

[Mean and standard deviation are denoted by μ and σ, respectivley.]

Temperature, °C	Load, g	Depth below surface, μm									
		150		100		75		50		25	
		Backthinning rosette diameter, μm									
		μ	σ	μ	σ	μ	σ	μ	σ	μ	σ
750	100	0	0	0	0	181	5.0	379	11.2	396	9.5
700	500	0	0	703	21.4	726	25.8	745	15.2	728	26.5
	300	0	0	0	0	589	40.9	607	9.7	594	9.0
	100	0	0	0	0	147	4.5	308	13.4	327	13.5
650	100	0	0	0	0	0	0	346	9.1	214	10.1
600	500	0	0	0	0	232	2.7	339	39.2	339	12.4
	300	0	0	0	0	158	10.0	202	5.6	258	12.1
	100	0	0	0	0	0	0	0	0	133	6.5
500	500	0	0	0	0	0	0	0	0	148	4.7
	300	0	0	0	0	0	0	0	0	104	3.8
	100	0	0	0	0	0	0	0	0	0	0

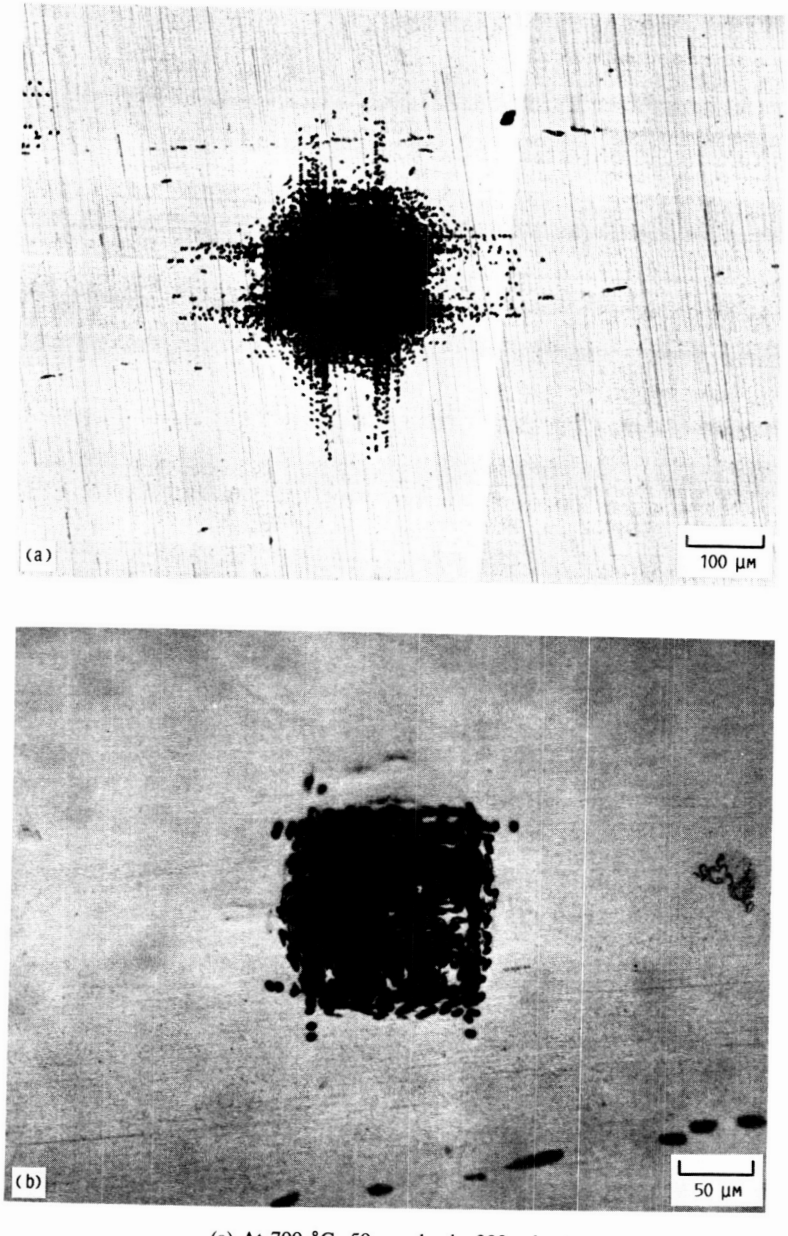

(a) At 700 °C, 50-μm depth, 300-g load.
(b) At 700 °C, 75-μm depth, 100-g load.

Figure 17.—Dislocation rosettes below surface revealed by etching.

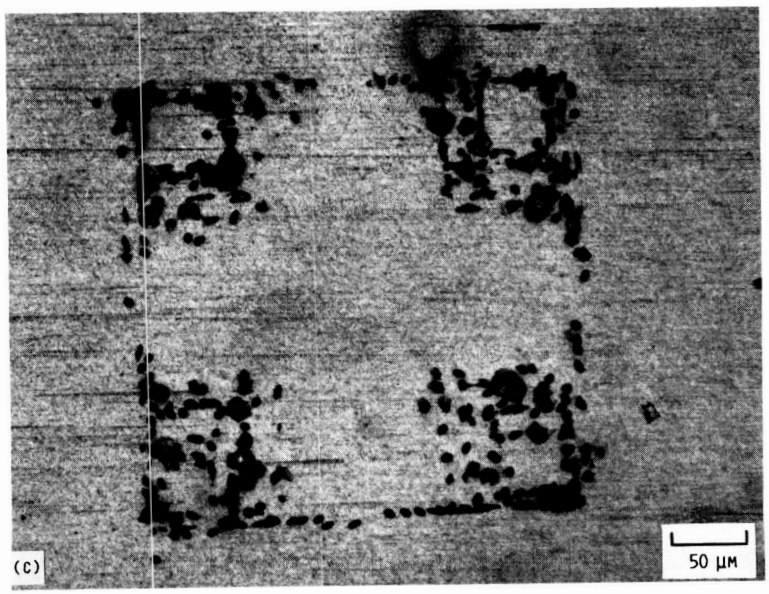

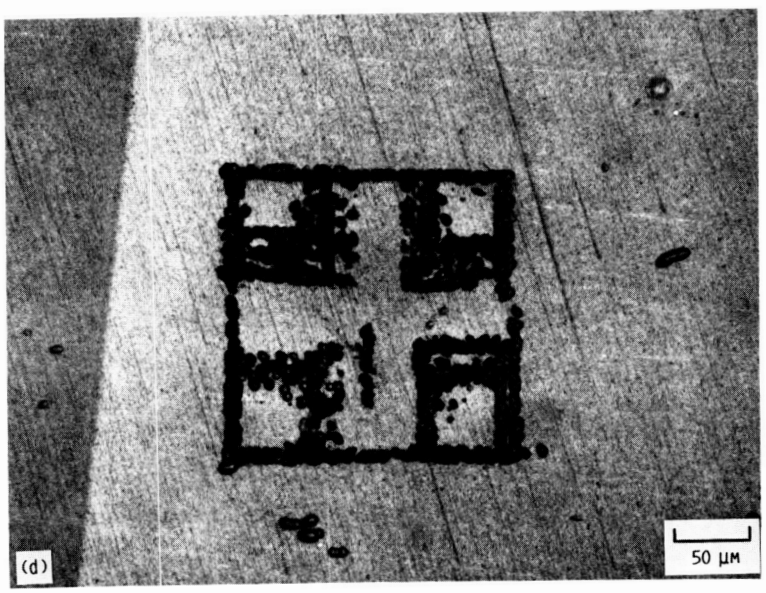

(c) At 700 °C, 150-μm depth, 300-g load.
(d) At 600 °C, 100-μm depth, 500-g load.

Figure 17.—Continued.

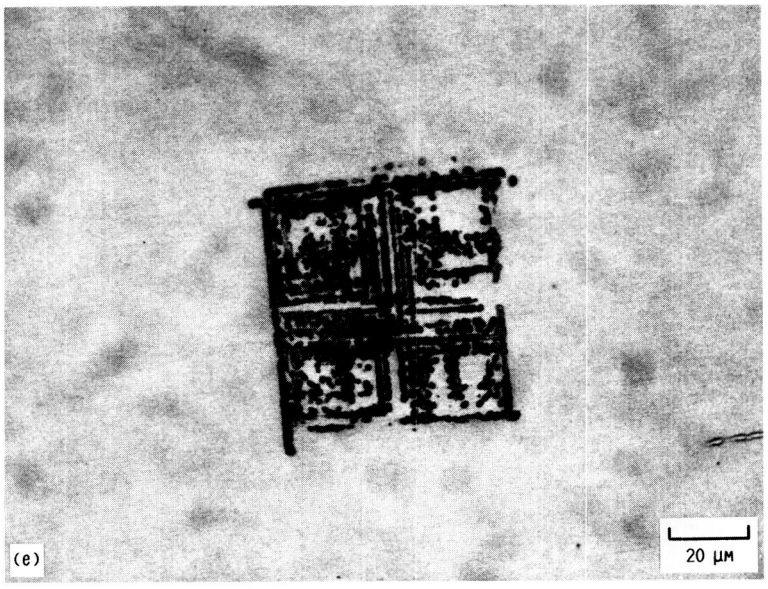

(e) At 600 °C, 50-μm depth, 100-g load.
(f) At 500 °C, 50-μm depth, 100-g load.

Figure 17.—Concluded.

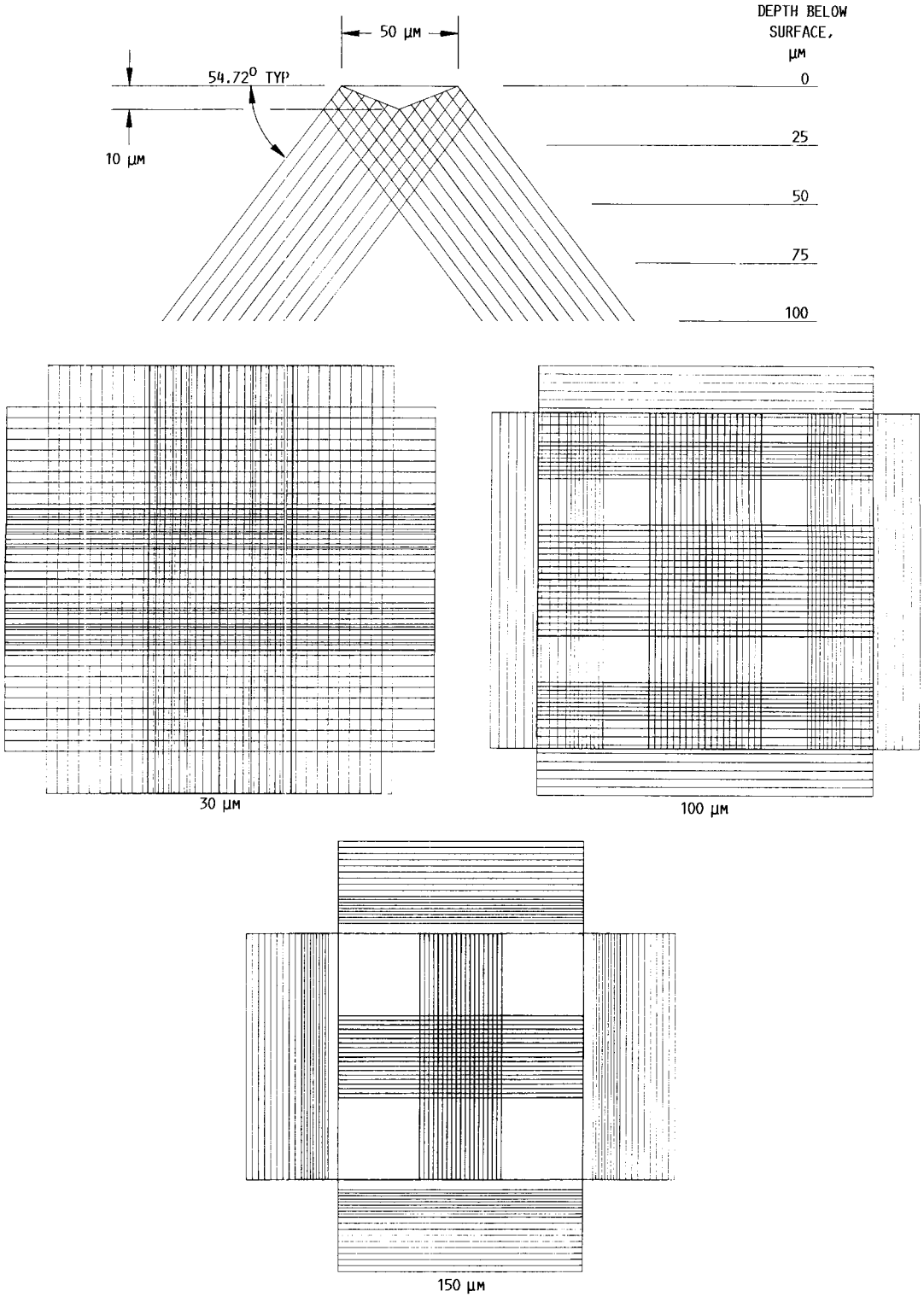

Figure 18.—Schematic of dislocation reactions below indent.

Figure 18 is a schematic diagram of these interactions. From this diagram it can be seen that any given (111) plane below the indent can intersect many other {111} planes. The multiple number of planes gives the dislocations many opportunities for interaction. The lower inserts in figure 18 are sections through the drawing at 50, 100, and 150 μm below the surface. Although they are provided just as examples and do not take into account the actual indent sizes or width-to-depth ratios, they provide a qualitative picture of what might be expected in backthinning experiments. At 50 μm below the indent, many slip planes are intersected by the section, and the etch pit density is high. At 100 μm below the surface, fewer slip lines are present in the section below the indent, and thus less area of the plastic zone is populated with etch pits. At 150 μm below the indent, an even smaller fraction of the plastic zone is expected to be populated, and this again is observed. In the last two drawings, 100 and 150 μm below the surface, the intersections of the slip planes (which are center areas crossed by vertical and horizontal lines in these drawings) are the areas free of etch pits in the micrographs. Presumably this is a result of interactions of dislocations on these intersecting planes. Outside of these regions dislocation etch pits are observed.

Dislocations may react on the {111} planes in the plastic zone below the indent. The reactions can occur if the dislocations are dissociated or undissociated. The undissociated dislocations are of the type $1/2\langle 110\rangle$ and lie on {111} planes. Partial dislocations are of the type $1/6\langle 112\rangle$. Dislocations will react only if the magnitude of the resultant Burgers vector, and thus the dislocation energy, is reduced. Formation of Lomer or Lomer-Cottrell locks satisfies this criterion. Reaction of undissociated dislocations results in the formation of a Lomer lock. Reaction of undissociated dislocations results in the formation of a Lomer-Cottrell lock. This results in the formation of a dislocation with its Burgers vector out of the glide plane of either of the glide planes of the partials that formed it. It is a sessile dislocation and cannot move conservatively. This may be one reason why dislocation etch pit density falls with depth below the surface. Many dislocations may be pinned near the surface because of the formation of Lomer locks. In other cases dislocations of opposite signs may meet on intersecting {111} planes and annihilate each other.

Figure 17(f) shows the structure below an indent made at 500 °C and 50-μm depth. No plastic zone is visible. This is the only case in which cracks can be seen below the surface; they are probably the same cracks viewed from the surface, the deep median cracks.

Concluding Remarks

The following conclusions can be made:

1. Doping of silicon affects the hardness to a small extent. Intrinsic silicon is the hardest followed by the *p*-type material. The *n*-type silicon is the softest. This is consistent with the effect of doping on dislocation mobility: *n*-type doping provides the greatest increase in dislocation mobility. The effect was greatest above 500 °C, and the amount of difference decreased with falling temperature. Lower loads produced higher hardnesses because of recovery of the indent experienced at low loads.

2. Doping has an effect on the ductile-brittle transition temperature. The *p*-type doping reduced the DBTT by 15 °C, and the *n*-type doping reduced the DBTT by 35 °C. This is again consistent with the effect of doping on dislocation mobility.

3. DBTT is not affected by raising the load from 100 to 200 g and is thus independent of load as would be expected.

4. No effect of doping on the fracture toughness can be observed by this technique.

5. Doping does affect dislocation mobility as measured by rosette diameters: *p*-type silicon produces the longest rosettes, followed by intrinsic, and then *n*-type. The effect of *n*-type doping on dislocation mobility is at odds with the effect of doping on the DBTT. This contradiction may be associated with the effect of *n*-type doping on the effectiveness of the etching.

6. Increasing load increases rosette diameters and the size of the plastic zone. The effect is a little less than the effect of load on indentation diagonal on the surface and about in line with the effect below the surface.

7. Dislocations in the plastic zone under the indent react with each other, and the effect is a reduction in the dislocation density in the plastic zone with depth. Dislocations may react with each other to form Lomer or Lomer-Cottrell locks, and these may serve to nucleate cracks. Dislocations of opposite signs on intersecting planes may also be reacting to annihilate each other.

The effect of doping on the ductile-brittle transition temperature in silicon has been demonstrated by microhardness techniques. Many opportunities for further research remain. In this work heavier indenter loads were used to promote reproducible cracking. This may have obscured the effect of doping on hardness. Research into effects of doping on hardness at lower loads may provide a better demonstration of this effect. This research should be supplemented by other methods of evaluating the effect of doping, such as the effect of doping on the DBTT as determined by the four-point bending method. The results could then be compared and contrasted. TEM examination of the indented zone could also provide insight into the mechanism of the DBTT. Etch pitting of the dislocation rosettes did not provide the expected results in the case of *n*-type doping. Other etchants and techniques for measuring dislocation activity might reveal the expected effects. Electron beam induced contrast (EBIC) is one promising technique for use in these studies. Finally, research into the effect of doping on other semiconductors, such as silicon carbide, should be conducted to investigate the effect of doping on the DBTT in other materials.

Lewis Research Center
National Aeronautics and Space Administration
Cleveland, Ohio 44135, August 17, 1988

References

1. Dieter, G.E.: Mechanical Metallurgy, 2nd ed., McGraw Hill, 1976, p. 396.
2. Yoffe, E.H.: Elastic Stress Field Caused by Indenting Brittle Materials. Philos. Mag. A, vol. 46, no. 4, Oct. 1982, pp. 617–628.
3. Hill, R.: Mathematical Theory of Plasticity, Clarendon Press, Oxford, 1950, p. 97.
4. Breval, E.; and MacMillan, N.H.: Elastic Recovery at Vickers Hardness Impressions. J. Mater. Sci. Lett., vol. 4, no. 6, June 1985, pp. 741–742.
5. Henshall, J.L.; and Brookes, C.A.: Measurement of K_{IC} in Single Crystal SiC Using the Indentation Method. J. Mater. Sci. Lett., vol. 4, no. 6, June 1985, pp. 783–786.
6. Palmqvist, S.: Rissbildungsarbeit bei Vickers-Eindruecken als Mass fuer die Zaehigkeit von Hartmetallen. Arch. Eisenhuettenwesen, vol. 33, no. 9, Sept. 1962, pp. 629–634.
7. Niihara, K.: A Fracture Mechanics Analysis of Indentation Induced Palmqvist Crack in Ceramics. J. Mater. Sci. Lett. vol. 2, no. 5, May 1983, pp. 221–223.
8. Evans, A.G.; and Charles, E.A.: Fracture Toughness Determinations by Indentation. J. Am. Ceram. Soc., vol. 59, no. 7–8, July–Aug. 1976, pp. 371–372.
9. Danyluk, S.; Lim, D.; and Kalejs, J.: Microhardness of Carbon-Doped (111) P-type Czochralski Silicon. J. Mater. Sci. Lett., vol. 4, no. 9, Sept. 1985, pp. 1135–1137.
10. Lawn, B.; and Marshall, D.: Hardness, Toughness, and Brittleness Indentation Analysis. J. Am. Ceram. Soc., vol. 62, no. 7–8, July–Aug. 1975, pp. 347–350.
11. Anstis, G., et al.: A Critical Evaluation of Indentation Techniques for Measuring Fracture Toughness. I—Direct Crack Measurements. J. Am. Ceram. Soc., vol. 64, no. 9, Sept. 1981, pp. 533–538.
12. Roberts, S.G.; Pirouz, P.; and Hirsch, P.B.: A Simple Technique for Measuring Doping Effects on Dislocation Motion in Silicon. J. De Physique, vol. 44, no. C-4, 1983, pp. 75–83.
13. Hu, S.: A Method for Finding Critical Stresses of Dislocation Movement. Appl. Phys. Lett., vol. 31, no. 3, Aug. 1, 1977, pp. 139–141.
14. Hirth, J.P.; and Lothe, J.: Theory of Dislocations, 2nd Ed., Wiley, 1982, p. 373.
15. Cockayne, D.J.H.; Ray, I.L.F.; and Whelan, M J.: Investigations of Dislocation Strain Fields Using Weak Beams. Philos. Mag., vol. 20, no. 168, Dec. 1969, pp. 1265–1270.
16. Hirsch, P.B.: Electronic and Mechanical Properties of Dislocations in Semiconductors. Defects in Semiconductors, J. Narayan and T.Y. Tan, eds., Elsevier, 1981, pp. 257–271.
17. Pirouz, P.: Deformation Mode in Silicon, Slip or Twinning? Scripta Met., vol. 21, no. 11, Nov. 1987, pp. 1463–1468.
18. Wessel, K.; and Alexander, H.: On the Mobility of Partial Dislocations in Silicon. Philos. Mag., vol. 35, no. 6, June 1977, pp. 1523–1536.
19. Patel, J.R.; and Chaudhuri, A.R.: Charged Impurity Effects on the Deformation of Dislocation-Free Germanium. Phys. Rev., vol. 143, no. 2, Mar. 1966, pp. 601–608.
20. Kulkarni, S.B.; and Williams, W.S.: Dislocation Velocities and Electronic Doping in Silicon. J. Appl. Phys., vol. 49, no. 10, Oct. 1976, pp. 4318–4324.
21. Roberts, S.G.; Pirouz, P.; and Hirsch, P.B.: Doping Effects on Indentation Plasticity and Fracture in Germanium. J. Mater. Sci., vol. 20, no. 5, May 1985, pp. 1739–1747.
22. Hirsch, P.B., et al.: Indentation Plasticity and Polarity of Hardness on (111) Faces of GaAs. Philos. Mag. B., vol. 52, no. 3, Sept. 1985, pp. 759–784.
23. Frisch, H.L.; and Patel, J.R.: Chemical Influence of Moles and Electrons on Dislocation Velocity in Semiconductors. Phys. Rev. Lett., vol. 18, no. 19, May 8, 1967, pp. 784–787.
24. Haasen, P.: Electronic Processes at Dislocation Cores and Crack Tips. Atomistics of Fracture, NATO Conference Series VI, R.M. Latanision and J.R. Pickens, eds., Plenum Press, 1983, pp. 707–730.
25. Jones, R.: The Structure of Kinks on the 90° Partial in Silicon and "A Strained-Bond Model" for Dislocation Motion. Philos. Mag. B., vol. 42, no. 2, Aug. 1980, pp. 213–219.
26. Warren, P.D.; Pirouz, P.; and Roberts, S.G.: Simultaneous Observation of α and β-Dislocation Movement and Their Effect on the Fracture Behavior of GaAs. Philos. Mag. A., vol. 50, no. 5, Nov. 1984, pp. L23–L28.
27. Samuels, J., et al.: A TEM Investigation of the Plastic Zone, Dislocation Rosettes and Cracks Around Vickers Indentations in Silicon. Microscopy of Semiconductor Materials 1985, A.G. Gullis and D.B. Holt, eds., Adam Hilger, 1985, pp. 49–54.
28. Kelly, A.; Tyson, W.R.; and Cottrell, A.H.: Ductile and Brittle Crystals. Philos. Mag., vol. 15, no. 135, Mar. 1967, pp. 567–586.
29. Burns, S.J.: Crack Tip Dislocation Nucleation Observations in Bulk Specimens. Scripta Met., vol. 20, no. 11, Nov. 1986, pp. 1489–1494.
30. Rice, J.R.; and Thompson, R.: Ductile Versus Brittle Behaviour of Crystals. Philos. Mag., vol. 29, no. 1, Jan. 1974, pp. 73–97.
31. Ohr, S.M.: Electron Microscope Studies of Dislocation Emission From Cracks. Scripta Met., vol. 20, no. 11, Nov. 1986, pp. 1501–1505.
32. Li, J.C.M.: Computer Simulation of Dislocations Emitted From a Crack. Scripta Met., vol. 20, no. 11, Nov. 1986, pp. 1477–1482.
33. Anderson, P.M.; and Rice, J.R.: Dislocation Emission From Cracks in Crystals or Alloy Crystal Interfaces. Scripta Met., vol. 20, no. 11, Nov. 1986, pp. 1467–1472.
34. Michot, G.; and George, A.: Dislocation Emission From Cracks—Observations by X-Ray Topography in Silicon. Scripta Met., vol. 20, no. 11, Nov. 1986, pp. 1495–1500.
35. Ashby, M.F.; and Embury, J.D.: The Influence of Dislocation Density on the Ductile-Brittle Transition in BCC Metals. Scripta Met., vol. 19, no. 4, Apr. 1985, pp. 557–562.
36. St. John, C.: The Brittle to Ductile Transition in Pre-Cleaved Silicon Single Crystals. Philos. Mag., vol. 32, no. 6, Dec. 1975, pp. 1193–1212.
37. Hirsch, P.B.; Roberts, S.G.; and Samuels, J.: The Dynamics of Dislocation Generation at Crack Tips and the Ductile Brittle Transition. Scripta Met., vol. 21, no. 11, Nov. 1987, pp. 1523–1528.
38. Behrensmeier, R.; Brede, M.; and Haasen, P.: The Influence of Precipitated Oxygen on the Brittle Ductile Transition of Silicon. Scripta Met., vol. 21, no. 11, Nov. 1987, pp. 1581–1585.
39. Sylwestrowicz, W.D.: Mechanical Properties of Single Crystals of Silicon. Philos. Mag., vol. 7, no. 83, Nov. 1962, pp. 1825–1845.
40. Puttick, K.E.: The Correlation of Fracture Transitions. J. Phys. D: Appl. Phys., vol. 13, no. 12, Dec. 14, 1980, pp. 2249–2262.

NASA
National Aeronautics and Space Administration

Report Documentation Page

1. Report No.	2. Government Accession No.	3. Recipient's Catalog No.
NASA TP-2863		

4. Title and Subtitle	5. Report Date
Indentation Plasticity and Fracture in Silicon	November 1988
	6. Performing Organization Code

7. Author(s)	8. Performing Organization Report No.
George C. Rybicki and P. Pirouz	E-4184
	10. Work Unit No. 505-63-1A

9. Performing Organization Name and Address	11. Contract or Grant No.
National Aeronautics and Space Administration Lewis Research Center Cleveland, Ohio 44135-3191	13. Type of Report and Period Covered Technical Paper

12. Sponsoring Agency Name and Address	14. Sponsoring Agency Code
National Aeronautics and Space Administration Washington, D.C. 20546-0001	

15. Supplementary Notes

George C. Rybicki, NASA Lewis Research Center; P. Pirouz, Case Western Reserve University, Department of Materials Science and Engineering, Cleveland, Ohio 44106. This report was a thesis submitted by George C. Rybicki as partial fulfillment of the requirements for the degree Master of Science to Case Western Reserve University in May 1988.

16. Abstract

Measurements of the ductile-brittle transition temperature (DBTT) of heavily doped silicon were obtained by using indentation techniques. Diamond pyramid hardness tests were performed on the (100) face of heavily doped *n*-type and *p*-type and intrinsic silicon single crystals. Tests were performed at 200 to 850 °C with loads of 100 to 500 g. Samples were subsequently etched to reveal dislocation rosettes produced by indentation. Intrinsic silicon underwent a ductile-brittle transition at 660 °C, *p*-type at 645 °C, and *n*-type at 625 °C. Hardness values varied from 1.1 GPa at 700 °C to 11.7 GPa at 200 °C. Significant effects of hardness on doping were present only at the highest temperatures. Lower loads generally produced higher hardness, but load did not affect the DBTT. Fracture toughness values ranged from 0.9 MPa $m^{1/2}$ at 200 °C to 2.75 MPa $m^{1/2}$ near the DBTT. Doping did not affect the fracture toughness of silicon. The *p*-type doping increased the size of dislocation rosettes observed after indentation, but the *n*-type did not, in contradiction of the expected results. Results are discussed in terms of the effect of doping on the dislocation mobility in silicon.

17. Key Words (Suggested by Author(s))	18. Distribution Statement
Silicon; Ductile-brittle transition temperature; Dislocations; Hardness; Fracture toughness	Unclassified – Unlimited Subject Category 26

19. Security Classif. (of this report)	20. Security Classif. (of this page)	21. No of pages	22. Price*
Unclassified	Unclassified	32	A03

NASA FORM 1626 OCT 86

*For sale by the National Technical Information Service, Springfield, Virginia 22161

NASA-Langley, 1988